

UNIVERSIDAD CARLOS III DE MADRID
ESCUELA POLITÉCNICA SUPERIOR



Bachelor Thesis

**ASSEMBLY, MODELING, SIMULATION AND
CONTROL OF A QUADCOPTER FOR
APPLICATION TO SOLAR FARM
INSPECTION**

September, 2015

A bachelor thesis submitted in fulfillment of the requirements for
the degree in Aerospace Engineering

Author: Maite Arteta Fernández

Tutor: David Morante González

Director: Manuel Soler Arnedo

Contents

1	Introduction	1
1.1	History	1
1.2	Socioeconomic framework	2
1.3	Legal framework	2
1.4	Personal motivation	3
1.5	Goals	3
1.6	Methodology	4
1.7	Time planning	4
1.8	Structure	6
2	State of the art, selection process and discussion of alternatives	7
2.1	State of the art	7
2.1.1	Software	8
2.1.2	Hardware	9
2.2	Selection process	9
2.2.1	Specifications	9
2.2.2	Type of vehicle	10
2.2.3	Board	10
2.2.4	Frame	11
2.2.5	Motors	11
2.2.6	Electronic Speed Controller	12
2.2.7	Blades	13
2.2.8	GPS	14
2.2.9	Battery	15
2.2.10	Receiver and transmitter	17
3	Assembly and installation	19
3.1	Hardware	19
3.1.1	ESC's and battery soldering	20
3.1.2	Arm assembly	20
3.1.3	Motor mount-assembly	21
3.1.4	Blades selection and assembly	22
3.1.5	Upper board assembly	22
3.1.6	GPS, receiver and APM assembly	22
3.1.7	Vehicle's wiring	23
3.2	Software	26
3.2.1	Computer preparation	26

3.2.2	UAV's configuration	26
3.2.3	Configuration of the PIDs	31
4	Modeling	35
4.1	Theoretical background	35
4.1.1	Reference frames	35
4.1.2	Equations of motion	36
4.2	Estimation of drag and thrust coefficients	38
4.3	Test bench setup	38
4.4	Test bench results	39
4.5	Estimation of mass and inertial properties	41
4.5.1	Use of commercially available CAD tool	41
5	Simulink modeling	43
5.1	State space modeling	43
5.2	Simulink model	45
5.3	PIDs	46
5.3.1	PID tuning	47
6	Experimental results	51
6.1	Software familiarization	51
6.2	Vehicle capabilities	54
6.3	Data retrieving	54
6.4	Logs analysis	55
7	Results	57
7.1	Experimental PIDs in Simulink	57
7.2	Theoretical PIDs in Vehicle	61
8	Conclusions	65
8.1	Future work	66
	Bibliography	67
	Appendices	69
	A Aerodynamic Forces and Moments	70
	B Test bench data	73
	C Mass of the components	75
	D SolidEdge plans with dimensions	76
	D.1 Draft of arm	77
	D.2 Draft of upper frame board	78
	D.3 Draft of lower frame board	79
	E 3-D printing	80
	F Simulink dynamic model	82

List of acronyms

UAV : Unmanned Aerial Vehicle

UAS : Unmanned Aerial System

MAV : Micro Aerial Vehicle

SUA : Small Unmanned Aircraft

DIY : Do It Yourself

RTF : Ready To Fly

APM : ArduPilot Mega

IMU : Inertial Measurement Unit

DC : Direct Current

ESC : Electronic Speed Controller

GPS : Global Positioning System

PID : Proportional Integral Derivator

List of Figures

1.7.1 Diagram of Gantt	5
2.1.1 Example of SUAs	8
2.1.2 Processor boards	9
2.2.1 Frame of the quadcopter	11
2.2.2 Brushless motors	12
2.2.3 Electronic Speed Controllers of the quadcopter	13
2.2.4 Blade of quadcopter	14
2.2.5 GPS of the quadcopter	15
2.2.6 Diagram battery	15
2.2.7 Battery of the quadcopter	16
2.2.8 Receiver and transmitter of the quadcopter	17
3.1.1 Battery , battery and lower frame board soldering	20
3.1.2 Arms screwed to the lower frame board	21
3.1.3 Motor-back view	21
3.1.4 ESC's and motor wiring	22
3.1.5 Blades configuration	22
3.1.6 Damping cushions	23
3.1.7 GPS wiring	23
3.1.8 Receiver wiring	24
3.1.9 ESCs wiring	24
3.1.10 Vehicle's wiring © Jethro Hazelhurst / DIYDRONES	25
3.2.1 Vehicle type selection	26
3.2.2 Frame type selection	27
3.2.3 COM port selection	27
3.2.4 Accelerometer calibration	28
3.2.5 Battery configuration	29
3.2.6 Radio calibration	29
3.2.7 Flight modes selection	30
3.2.8 Mission Planner motor interface	31
3.2.9 Quadcopter PID tuning loop	32
3.2.10 Indoor flight structure	33
4.1.1 Frames of the vehicle	36
4.1.2 Aerodynamic moments	37
4.3.1 Test bench setup	39
4.4.1 Momentum (M_j) vs. Ω^2	40

4.4.2 Thrust (T_j) vs. Ω^2	40
4.5.1 SolidEdge drone model	42
5.2.1 Simulink system inputs	45
5.2.2 Variation of ω with respect to <i>throttle</i>	46
5.3.1 PID scheme	47
5.3.2 Roll PID tuning	48
5.3.3 Pitch PID tuning	49
5.3.4 Yaw PID tuning	49
6.1.1 Mission planner Flight Data	52
6.1.2 Mission Planner Flight Plan	52
6.1.3 Mission Planner Configuration/Tuning	53
6.1.4 Mission Planner Terminal	54
6.3.1 Data retrieving	55
6.4.1 Logs interface	56
7.1.1 Roll results	58
7.1.2 Pitch results	59
7.1.3 Yaw results	60
7.2.1 Roll results	62
7.2.2 Pitch results	63
7.2.3 Yaw results	64
E.0.1 Included logotypes	80
E.0.2 3D printed quadcopter	81
F.0.1 Quadcopter Simulink model	83
F.0.2 PD controller	84
F.0.3 Quadcopter dynamics	85
F.0.4 Omega calculator block	86
F.0.5 Angle's block	87
F.0.6 Displacement block	88

List of Tables

1.1	Unmanned Aerial Vehicles current applications	2
2.1	Comparison of the different vehicle configurations	10
2.2	Comparison of the different processor boards	10
2.3	Brushed and brushless motors comparison	12
2.4	Comparison of different blade materials	14
2.5	Comparison different types of batteries	16
2.6	Characteristics of the battery	17
3.1	Kit components	19
3.2	PID values	34
4.1	Graphs parameters	41
4.2	Moments of inertia obtained from CAD drawing	42
5.1	Effects of increasing each parameter	46
B.1	Data to obtain C_T	73
B.2	Data to obtain C_D	74
C.1	Kit components	75

Notation

ϕ, θ, ψ : Euler angles

I_{xx}, I_{yy}, I_{zz} : Moments of inertia

I_{xy}, I_{xz}, I_{yz} : Products of inertia

Ω_i : Angular velocity of blade i

l : Arm's longitude

Q_i : Drag of blade i

A : Blade's cross section

m : Mass of the quadcopter

g : Gravity

C_D : Drag coefficient

C_T : Thrust coefficient

M_j : Torque

K_P, K_D, K_I : Proportional, Derivative and Integrator gain

e : Error

T : Kinetic energy

V : Potential energy

Acknowledgments

First of all I would like to thank my family who have always supported me and encouraged to keep aiming higher.

Secondly I would like express my gratitude to Manuel Soler Arnedo and David Morante González for giving me the idea of undertaking a project in such emerging field and also for giving me support and comprehension through our weekly meetings.

Thirdly I would like to thank Gonzalo Sanchez Arriaga for providing me with the dynamic model of the quadcopter and also for providing me academic support every time I needed it.

Also I would like to highlight the work of Carlos Cobos Pérez who has been the artifice of overcoming the logistical problems in the laboratory.

Last but not least I would like to thank Lucía Muñoz Córdoba and Diego Provencio Moreno for being the best 'lib&lab buddies' I could have never asked for. You have made this much more entertaining.

Abstract

Unmanned Aerial Vehicles (UAV) have been utilized for multiple purposes during the last century. Even though their beginning was clearly militarized, they constitute a field that has evolved and has adapted itself to the population's current needs. Since 2005 the world is starting to experience a thrilling growth in the use of Unmanned Aircraft Systems as the technology with the potential to make possible new civilian applications. In an attempt of unifying the two most popular concerns nowadays, renewable energies and unmanned vehicles, this bachelor thesis is presented. The final goal is to assemble and configure one vehicle from scratch to allow it to be used in the future for solar panel inspection. For that instance, the project is divided in three main parts. In the first section, a research in the current market is carried out, taking into account the current legislation, to find the most suitable components for the UAV. After the components are ordered and received, the second part can be said to start. In it, the process is divided into two assembly processes. On one hand, at the physical level, the pieces are brought together by means of soldering, wiring and screwing. On the other hand, at the software level, the vehicle's processor is configured with the aid of a compatible free source software. Afterwards, in an attempt of stabilizing the platform, its PIDs are tuned in. Regarding the third part, the vehicle is modeled by means of a physical characterization that allows to obtain its main performance coefficients and inertial properties. Moreover, a set of dynamic equations are proposed to comply with the real behavior, and a set of PID parameters are proposed to be the UAV stabilizing parameters. Furthermore, the PID sets obtained in parts 2 and 3 are compared in order to clarify which one is more suitable.

Keywords: UAV, assembly, physical characterization, modeling, control

Chapter 1

Introduction

This chapter familiarizes the reader with the emerging field of unmanned vehicles through the reviewing of their history and their implications at the current legislative and socioeconomic levels. Furthermore, the personal motivation which was triggered by the previously mentioned factors is presented. Moreover, in an attempt to ease the bachelor thesis reading, the structure along with the objectives to be achieved are introduced.

1.1 History

Although the popular belief in which the unmanned aerial vehicles are a relatively recent invention dating back to at most thirty years, these vehicles go back to ancient times. The oldest registered data date from 1849 when the Austrian army used balloons armed with explosives against the city of Venecia. Even though, nowadays balloons are left out of the current UAV category, they were close to the concept of an unmanned platform carrying a payload. As it can be deduced from the previous historical fact, technology and more specifically drones emerged to address a need of improvement, to meet the current needs and sometimes to surprise and conquer the contrary. Moreover, these vehicles quickly developed during war periods, in which instilling the contrary was a must. During the First World War, the first pilotless aircraft were built and the radio control techniques were mastered to the point at which they were able to carry and guide missiles to the desired aims. Even though remotely piloted aircraft were also included as part of military weapons during the Second World War, it was not until the 90's when they reached their peak. During this period, unmanned aerial vehicles, which had been perfected during the previous decade, were used as tools to watch and film the targets and to ultimately neutralize them. Consequently, the inclusion of these remotely piloted vehicles in war times has become vital , Irak war, Syria war...

However, despite their clear military purpose in the olden times, since 2005 the world is starting to experience a thrilling growth in the use of Unmanned Aircraft Systems as the technology with the potential to make possible new civilian applications. As a consequence, their application has been widened and they are playing an important role on missions with very different scopes as the ones shown in Table 1.1:



Scope	Mission
Security-related	Homeland security
Safety related	Civil Defense Fire Fighters
European union	Border Guards Police
Commercial Air Transport	Scheduled Air Service
General Aviation	Pleasure Corporate Operations Flight Training
Aerial Work	Advertising Survey and Mapping Photography Search and Rescue

Table 1.1: Unmanned Aerial Vehicles current applications

1.2 Socioeconomic framework

Due to the unstoppable inclusion of unmanned vehicles in quotidian activities at both governmental and non-governmental level, this industry has earned a positive image over the years and so far it has the sympathy and attention of the public. However, in order to ensure this acceptance, it is essential that the UAV industry reinforces the communication on their advantages their its eco-friendly development.

Regarding its market evolution, experts coincide that the current trend will not vary in the years to come, meaning that it will be still leaded by USA and followed by Europe and Asia. However, this situation may not be as durable as expected, countries where this market is starting to take off nowadays are believed to take over thanks to their untapped potential. As a consequence of this believed growth, a lot of new jobs will be created and the success of the market will depend on regulations to maintain acceptable market conditions.

According to analysis conducted by Inea Consulting Ltd¹, the current global market value under best case scenario will reach € 563.7 million in 2015 and is expected to continue its growth to € 612.9 million in 2016.

1.3 Legal framework

Due to this dramatic increase in their usage many organizations at both international and national level have been obliged to step forward to understand, define and ultimately reflect them in their legislation.

Regarding the Spanish legislation[1] , in order of defining the requirements that each vehicle has to comply with to be allowed to fly, these vehicles are divided in two main categories depending on their weights as follows:

1. MTOW below 25 kilograms: they are allowed to operate on the outskirts of cities and inhabited places at a maximum height of 120 meters and within the pilot's visual field. Moreover it is required to have optimum meteorological conditions.

¹www.commercialandciviluavmarketguide2015.com



2. MTOW over 25 kilograms: these kind of vehicles are used in fire extinguishing, rescue and search operations. Furthermore, they shall comply with specifications and limitations established in their Airworthiness Certificate issued by Agencia Estatal de Seguridad Aérea.

Despite the legislation introduced by every State within their territories it is indispensable that all the countries come together to elaborate a global and variant legislation to accommodate the UAS requirements in the years to come.

1.4 Personal motivation

Drones are a recurring issue as they are continuously appearing in the news along with their multiple applications in both the military field and the civilian. But even though their usage is widespread and they constitute a field that continuously evolves and aims to keep progressing, understanding and becoming familiar with its operating system and mechanisms are concerns that have been remained unsatisfied for long time.

Furthermore, in the past two decades, as a result of climate change, there has also been an exponential growth in the concern about the future of energy. Renewable energies have been presented as the solution to reduce greenhouse gas emissions and among all the sustainable energies, photovoltaics have become popular. This technology consists in converting solar radiation into electrical energy through a noise-free, environmentally friendly process. Nevertheless, the expansion in the usage of this source of energy has urged the necessity of exploring a reliable and cost-saving method for determining the performance and failure of the panels. For that instance, it is decided to assemble and configure an unmanned aerial vehicle from scratch which will be used in the future to inspect photovoltaic panels.

1.5 Goals

In this project the main objective is to predict the behavior of a quadcopter fully built and configured from scratch. However, this main objective implies some other ones to be accomplished, stated hereinafter:

1. Selection of the different parts that will form the vehicle, considering several alternatives and reasoning the selection of each element that finally composes the setup.
2. Start up and refinement of every component, such as calibrating the electronic speed controllers and the processor.
3. Stabilization of the vehicle through the tuning of its controller.
4. Design of the UAV by using Solid Edge to both characterize more accurately its moments of inertia and to allow a 3D printing of every non electronic piece.
5. Implementation of the vehicle's dynamics and mechanics in Simulink to predict its theoretical behavior.
6. Analysis and comprehension of the practical and theoretical results, with detailed reasoning and explanation of the observed consequences experienced by its exposure to different inputs.
7. Based on obtained results, suggest new ways to research into this field more deeply.



1.6 Methodology

In order to achieve the previously mentioned objectives, the methodology that will be followed consists in first doing an extensive market analysis that will drive the vehicle's selection. For that instance, an expert within the field will be contacted for advice. Since there are not many written references on how to mount quadcopters, mainly DIY blogs will be used in the documentation process before starting the assembly. In order to stabilize the vehicle it will be flown with different controller values until an almost no-perturbations flight is achieved. For that purpose, the Remotely Piloted Aircraft System (RPAS) will be attached to a metallic structure by means of strings and sliding rods which will allow it to climb. Regarding the theoretical part, Euler Lagrange will be utilized to obtain the equations of motion and a trial and error process will be carried out to guess the theoretical controller values.

1.7 Time planning

When dealing with such long time projects , time managing becomes crucial to avoid last minute changes and unpleasant surprises. For that reason a Gantt diagram in which deadlines are assigned to each milestone is created. Prior achieving a proper time organization, each objective was broken down into the necessary steps to fulfill them and it was analyzed how much time was expected to be spent in each section. However, as it can be seen from Figure 1.7.1, some unexpected events resulted in a delay that was finally resolved.



5

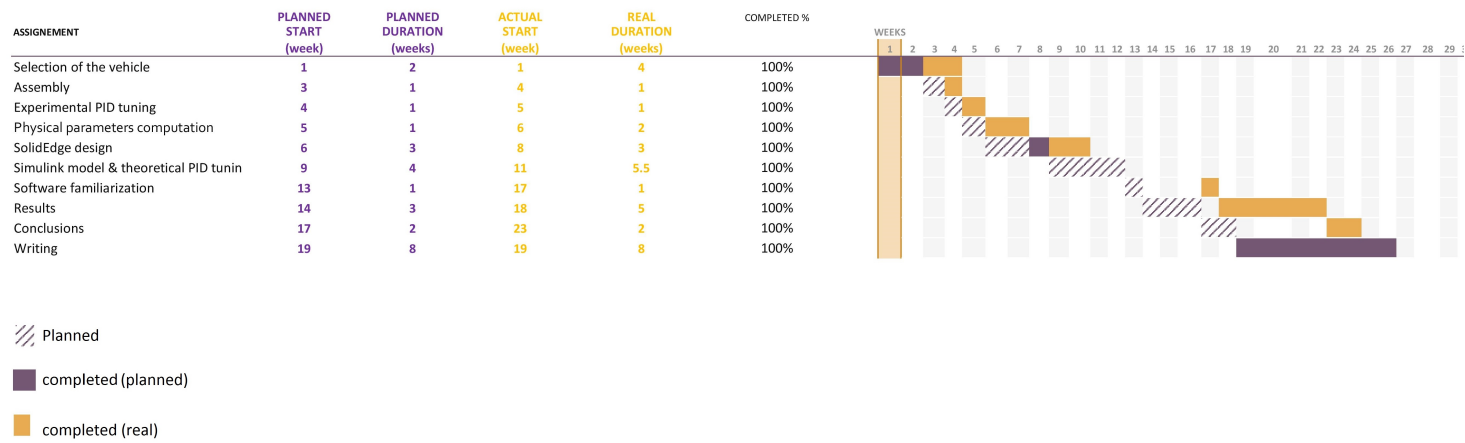


Figure 1.7.1: Diagram of Gantt



1.8 Structure

In an attempt to make the development of this final year project more coherent it will be structured according to the objectives. This implies the division of the text in 8 chapters.

1. In the second chapter, under the state of art the different categories in which these vehicles are grouped is presented and the different existing vehicles are introduced at both hardware and software levels. This section leads to an extensive reasoning of the elements that are needed to build our own vehicle and it drives the components election.
2. Within the third chapter, the reader will be able to undergo the whole assembly process through written instructions of the different steps. Furthermore, a manual tuning to stabilize the vehicle is attempted.
3. In the forth chapter the whole vehicle is drawn in SolidEdge with the aim of obtaining its moments of inertia and allowing 3D printing of replacement parts (Appendix E). Moreover a test bench will be set up to measure different physical parameters needed to characterize the quadcopter.
4. Through chapter 5 the dynamics of a quadcopters along with the physical characterization obtained in chapter 4 are implemented in Simulink to predict the theoretical behavior.
5. Chapter sixth is dedicated to help the reader have a deeper understanding in the data that is needed to simulate a flight and how to obtain and interpret it.
6. In the seventh chapter, two case scenarios are proposed to compare the behavior of the vehicle subjected to different controller values.
7. Finally, in chapter number eight the bachelor thesis' conclusions are presented along with some future work ideas.

Chapter 2

State of the art, selection process and discussion of alternatives

The concept of unmanned can lead to a general misunderstanding because while it is true that in the inside of the vehicle there is no one, there does exist a contact between the UAV and an Earth operator, which can either be a pilot or someone with the necessary skills. Due to this definition both aerostatic balloons and missiles are left out of this category. The selection of a vehicle is based on the objective and mission it has to fulfill and this choice will drive the UAV dimensions and the on board integrated technology. For instance, the number and size of the batteries will constrain the level of autonomy of the vehicle and the frequency of the controller will drive the maximum range of the drone. Primarily, owing to this emerging market, a necessity to sort them out in different categories depending on their size and weight has been created [2]:

- *Micro Air Vehicles (MAV)*: unmanned aircraft with a maximum length of 6 inches and a maximum weight of 0,22kg. MAVs tend to have several common characteristics: low Reynolds number, 3-7 lift to drag ratio range and 1-15 communication limit.
- *Small Unmanned Aircraft (SUA)*: these vehicles range from 0,5 to 25 kg gross weight. The 25 kg upper takeoff gross weight limit corresponds to the AMA upper weight limit for hobbyist aircraft. The new technologies offer SUAs the ability to carry high useful loads.

2.1 State of the art

In line with this project and according to the main purpose of the vehicle, inspection, that only requires it to carry a camera, the category that better fits it is SUA. By looking closer at this division a subcategory in which UAVs are categorized depending on its geometry is found. In this subcategory of multirotors the most common UAVs are encompassed under quadcopter, hexacopter and octocopter.

- *Quadcopter*: these vehicles possess 4 rotors for lifting and propelling and their movement is controlled by varying the relative thrust of each rotor. In order to avoid them from spinning around themselves two opposite lying rotors spin in one direction, while the other two opposite lying rotors spin in the opposite direction.
- *Hexacopter*: the most notable difference at the construction level between these vehicles and the previous category is the number of propellers that they include. Moreover, at the

performance level their stability is better and even though they lost one engine they could still land.

- *Octocopter*: they are propelled by eight rotors and they operate in a similar way as they previous cases. As a matter of fact, flight could continue after the loss of either one engine or two on opposite sides. They are mainly used for transportation of heavy objects due to their great stability.



Figure 2.1.1: Example of SUAs

2.1.1 Software

In pursuance of obtaining a total autonomous unmanned aerial vehicle capable of accomplishing the given mission, a complete symbiosis between the hardware and the software is needed. This important union leads to the so-called flight controllers which can be said to be the “neuralgic center” of the vehicle and the ones in charge of executing different orders. Their functioning combines the usage of both an algorithm or code integrated into a board to interpret and send orders, and a physical support to transfer these commands to the rest of the vehicle through their output PINS. Regarding software and property ownership concerns, two main categories are found: open source and proprietary software. The main difference is that while the first one provides the original source code to be used and to allow advanced users to introduce subsequent improvements , in the second case the software developer company owns it and gives the option to use it under some restricting conditions.

Although nowadays there are many available options in the market, the most popular hardware-software options are highlighted and analyzed below:

- *APM or ArduPilot Mega*¹: this processor is an open source project from 3DRobotics, and by default, very customizable. It began life as the Ardupilot for a fixed wing control system and quickly evolved to multicopters. During this growth it kept its compatibility with Arduino, making it by default be very personalizable. Furthermore, this board does not require any assembly.
- *PIXHAWK*²: this board has been shaped up to be the successor of the APM one due to its faster processor and its additional memory. Despite this, its main drawback is that it is has not been tested as much as the APM one. As a consequence, it is less reliable.

¹www.copter.com/apm26

²www.copter.com/pixhawk

- *NAZA*³: this frame is a non open source which means that unless a firmware update comes out its configuration would be all set up by the manufacturer. Beside this dissimilarity , the board does not include any other important feature that could make it outstand from the other models.

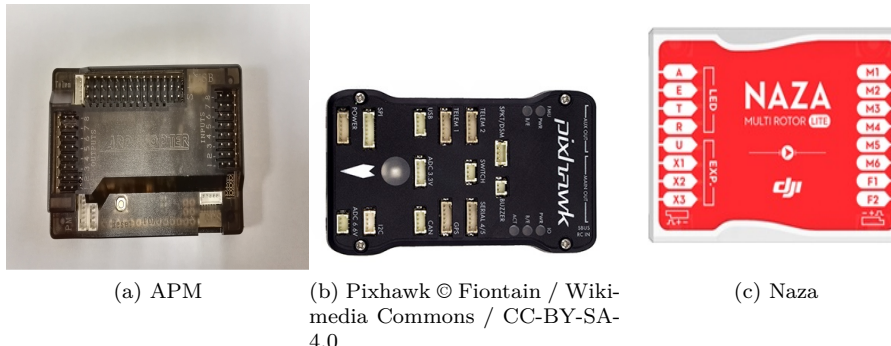


Figure 2.1.2: Processor boards

2.1.2 Hardware

The physical part of the drone consists of a robust structure that hosts the different controllers, and that possesses a rotor with an attached engine to each arm.

Doing a research in the current drone market, it is found that there are two available options that depend on the grade of assembly of the model. On one hand, , there exists a Do It Yourself (*DYI*) kit that includes the pieces needed for the model's assembly. The advantages are both its lower price and its ease to be customized by replacing some parts by others that would better meet the mission requirements. On the other hand, there exists a Ready To Fly (*FTR*) option which encloses all the already assembled units. Even though the price is higher this option does provide with an already operational vehicle ready to use.

Among the diversity in the RTF option there are some outstanding and popular models such as DJI Phantom, Parrot and Aeroquad.

2.2 Selection process

2.2.1 Specifications

Before entering into a detailed discussion about which components are selected and why it is believed that they are the most suitable for this project, it is highly desired to recall the mission that needs to be undertaken. For that instance, two main steps can be highlighted as they lead to the ultimate goal of inspecting any defects on the solar panels:

1. A thermal camera is added to an unmanned aerial vehicle for the purpose of inspecting and photographing solar panels.
 2. Once the vehicle has landed, those pictures are uploaded and examined in order to determine whether there is any anomaly in the solar panels.

³www.dji.com/naza



In order to fulfill this objective a set of requirements based on the bachelor thesis presented by *Román Esteban Hofer*[3] is proposed.

- *Weight*: it must not exceed 2kg.
- *Propulsion system*: the maximum thrust per motor has to be of 1 kg.
- *Flight controller*: it has to include an inertial measurement unit (IMU), a gyro stabilization, accelerometers, GPS, barometer and magnetometer.
- *Transmitter and receiver*: it must have at least four channels.
- *Budget*: the price must not exceed 400 Euros.

2.2.2 Type of vehicle

Knowing that the vehicle has to be compatible with any of the mentioned boards and before looking into any hardware components (Sub-Section 2.1.1) such as the vehicle frame or the controller, a type of vehicle has to be chosen. For this purpose, the most common vehicle configurations are analyzed ⁴ and compared in Table 2.1.

Characteristics	Quadcopter	Hexacopter	Octocopter
Overall price	LOW	MEDIUM	HIGH
Replacement price	LOW	MEDIUM	HIGH
Maneuverability	HIGH	MEDIUM	LOW
Landing after loss of one engine	NO	YES	YES
Payload that can be carried	LOW	MEDIUM	LARGE
Size	SMALL	MEDIUM	LARGE

Table 2.1: Comparison of the different vehicle configurations

Taking into account that the device will be flown in a controlled and hazard-free place it is assumed that no engine loss will occur and high maneuverability will be preferred. Besides this, the configuration choice is ease by the 400€-budget. As a consequence a quadcopter is determined to be the best option among other configurations.

2.2.3 Board

In order to chose a vehicle, the type of board to be integrated on board has been chosen from among all the above mentioned options (Sub-Section 2.1.1). To help decide a table gathering all the notable specifications has been built:

Board type	Open Source	Self leveling	Waypoint navigation	Position hold	Price
APM	YES	YES	YES	YES	\$200
PIXHAWK	YES	YES	YES	YES	\$320
Naza	NO	YES	NO	YES	\$300

Table 2.2: Comparison of the different processor boards

⁴www.dronebly.com

Given this context and due to the nature of this project, which implies great tracking and intervention in the operative system, it is concluded that the most suitable option is an open source environment that will delineate an effective path for the project development while allowing an efficient use of the given resources. Consequently, and provided that during the college degree Arduino has been introduced in some courses and laboratory sessions allowing the acquisition of certain knowledge about its programming methods, the upcoming project will be developed based on Arduino technology. Since both APM and PIXHWAK are similar and the only notable difference lies in the price, the APM board is chosen over the PIXHAWK one. However, it is advisable to take it into account in a future project as it is meant to be the successor of the APM board.

The main encountered difficulties reside in the fact that most of the Arduino-based drone projects are DIY and that there are not many drone specialized stores in Spain. Due to this, it is first considered the possibility of broadening the search to companies localized abroad. However, this idea is rejected because a closer back-up from the manufacturer is preferred.

2.2.4 Frame

The frame will be the physical support for the drone and to which all the other elements will be attached. Since there are numerous possibilities, in an attempt to narrow the quest, the choice will mainly depend on its size and material because they are the main parameters that drive the drone's weight and more specifically its performance. On one hand, , a heavy material could be detrimental as a higher force to lift it would be required. On the other hand, a low weighted material could be too fragile to withstand the multiple strokes it will receive when being tested. Also, it must be taken into account the material's flexibility: the higher it is the less damages would be caused in case it falls down. Due to this, two rigid metallic sheets are to be placed as the central structure to improve the drone's rigidity and to provide the board with a stable subjection. Concerning the arms of the drone four plastic branches are used in an X-configuration. The material selection lies in the capability of the plastic to absorb a great amount of vibrations and in its strength.



(a) Lower frame board (b) Upper frame board (c) Arms

Figure 2.2.1: Frame of the quadcopter

2.2.5 Motors

The motors election is very important as they need to be powerful enough to lift the whole drone. There are two main categories : brushed motors and brushless motors:

1. *Brushed motor*⁵: it is a Direct Current (DC) device that converts the electric energy into

⁵www.wikipedia.org/motor/escobillas



mechanic energy, resulting in a rotatory movement. They consist of a permanent magnet and a rotor with a set of windings. Brushed DC motors can be varied in speed by changing their strength or magnetic field or their voltage. Depending on the connections of the field to the power supply, their speed and torque characteristics can be altered to provide steady speed.

2. *Brushless motor*⁶: also known as electronically commutated motors, they are devices powered by a DC electric source via an inverter. This introduces the need of an electronic drive controller to generate torque, which means more complex and sometimes expensive systems. Within this motor category, two subcategories can be found: innerrunner and outrunners motors. The inner-rotor motors have much less magnetic material than the outer-rotor ones. This means that they are capable of less flux when the identical materials are used. However, its lower diameter they achieve a larger acceleration which can sometimes be beneficial.

Characteristics	Brushed motor	Brushless motor
Maintenance	PERIODIC	LESS
Efficiency	LOW, poor heat dissipation	HIGH
Electric Magnetic Interference	YES	ALMOST NONE
Electrical Speed Controller	NO	YES

Table 2.3: Brushed and brushless motors comparison

From Table 2.3 it can be summed up that the number of advantages of the brushless motors is greater than the ones of the brushed motors, hence the usage of brushless motors even though they can be a bit more expensive is convenient.



Figure 2.2.2: Brushless motors

2.2.6 Electronic Speed Controller

These devices are electronic circuits that essentially generate a three-phase electric source of energy. Their purpose is to vary the brushless motor's speed in a radio controlled model.

A regular ESC used for aeromodeling has five wires and three connectors used for different tasks:

⁶www.wikipedia.org/motor/sin/escobillas

- *Powering the ESCs:* two cables are connected to the battery and give enough energy to the ESCs to power them up.
- *Establishing the motors spin direction:* it consists in three connectors hooked to the three motor's wires by a three phase connection. The rotation direction will be determined by the order in which the wires are connected. In order to maintain a net aerodynamic torque and an angular acceleration equal to zero, two of the motors have to spin clockwise while the other do it counterclockwise.
- *Connecting the ESCs and the motors to the controller:* three cables (red, white and black) are connected to the microcontroller's PINs. In the simplest configuration, these cables will be used to both power and transmit the orders from the board to the motors. But if a power modulation was used, the board would receive the energy directly from the battery, only the white cable (the controller one) would be necessary.

In this case, since four motors will spin at different velocities four ESC's will be needed. It is recommended to use around 20 AMP- ESC's for quadrotors of around 1kg. Since this vehicle is believed to develop more complex missions in the future 30mAh ESCs are used instead .

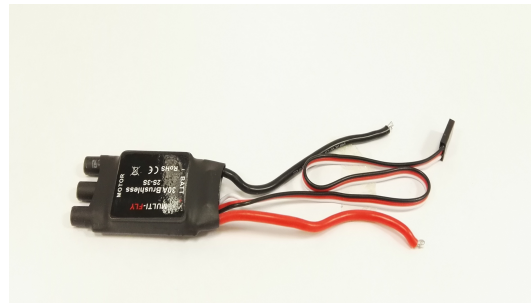


Figure 2.2.3: Electronic Speed Controllers of the quadcopter

2.2.7 Blades

A motor by itself is not able to specify the amount of thrust that it will generate. For that reason propellers need to be included. In order to select a suitable size for them, it must be taken into account that the torque constant and the voltage constant are related through a product that is kept constant for every motor : $KvKt = 1352$. As it can be seen from the formula Kv and Kt are inversely related, if one decreases the other one increases meaning that a small propeller would allow for greater speeds but reduced efficiency. In applications such this project, bigger propellers with lower speed but greater stability are preferable. Following the current's market trend 11 inches diameter blades will be used.

Once the size is figured out it is necessary to determine the material. Carbon Fiber, wood and plastic seem to be the most popular in the market⁷ and are analyzed to determine the one that better fits our design

⁷www.dronethusiast.com/blades

Features	Carbon Fiber	Wood	Plastic
Vibration	LOW	LOW	LOW
Weight	LIGHT	HEAVY	MEDIUM
Price	HIGH	HIGH	LOW
Thrust	MEDIUM	LOW	HIGH

Table 2.4: Comparison of different blade materials

From this table it can be seen that plastic propellers are the ones that better fit this project needs as its flexibility would allow them to absorb a shock and take up more easily any sudden changes in direction. On the contrary, if a carbon fiber one impacted , the motor bearing would take most of the impact. Regarding the wood propellers, they do not work well for acrobatics or stunt flying because of the increase in rotation momentum due to their heavier weight.

As mentioned before, 11 inch diameter blades are selected and from the materials comparison table it is determined that the best the material is plastic.



Figure 2.2.4: Blade of quadcopter

2.2.8 GPS

Global Positioning System is a system that allows to determine worldwide the position of an object. Their usage in UAVs is quite popular not only because of the positioning technology but also for their advanced technology that allow a drone to fly on its own with its flying destination or points pre-planned loaded into its operating system. Currently there are two features that are becoming more common, position hold-which lets the vehicle hold itself in a location in space and return to home- which makes the drone automatically return to the point from which it took off when signal is lost.

The vehicle's GPS is:



Figure 2.2.5: GPS of the quadcopter

2.2.9 Battery

Batteries are electrochemical devices consisting of two or more cells that convert stored chemical energy into electrical power. Each cell has a positive terminal, cathode, and a negative one, anode. In half of the cell, positively charged ions, cations, migrate to a cathode electrode through an electrolyte. In the other half of the cell, negatively charged ions, anions, migrate to the anode electrode through an electrolyte. A diagram that shows how they work can be found in Figure 2.2.6.

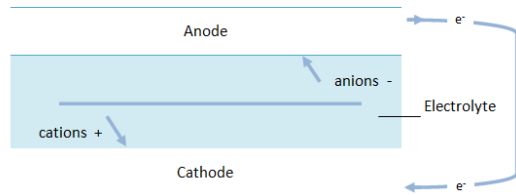


Figure 2.2.6: Diagram battery

Within this field, two types of batteries can be distinguished: rechargeable or single use. Beside the fact that the single use ones cannot be recharged, the non rechargeable ones usually have superior performance characteristics but the cost of replacing them after is that high that rechargeable ones are usually preferred. Moreover, when selecting a battery there are three important parameters that have to be taken into account:

1. Constant discharge current
2. Battery capacity



3. Battery voltage

After some research [4] several types of batteries have been found to be used for UAS propulsion systems in the last years. Their properties are shown in Table 2.5.

Battery type	Theoretical specific energy (W-hr/kg)	Practical specific energy (W-hr/kg)	Specific power (W/kg)	Cell voltage (V)
Ni-Cd	240	60	150	1.2
NiMH	470	23-85	200-400	0.94-1.2
Li-Ion	700	100-135	250-340	3.6
Li-Po	735	50.7-220	200-1900	3.7

Table 2.5: Comparison different types of batteries

Nickel Cadmium batteries (Ni-Cd) were dominant in the late 80s and 90s and were substituted by a brief appearance of Nickel metal hydride (NiMH) batteries in the early 2000s. However, Lithium-ion (Li-Ion) and lithium-ion-polymer (Li-Po) are the main type in use today for small UAS propulsion systems.

From Table 2.5, it is decided to use Li-Po batteries because they are the lightest ones and because thanks to their capability of providing with a great amount of energy they guarantee a longer flight.

Within the Li-Po battery options, the most suitable battery is the 11.1V 2600mAh 30C 28.86Wh MAXPRO LiPo.



Figure 2.2.7: Battery of the quadcopter

Number of cells	3
Dimensions (cm)	[10,1x3,5x3]
Capacity (mAh)	2600 mAh
Weight (g)	191
Maximum discharge intensity	2.6Ah
Charge intensity	2.6Ah

Table 2.6: Characteristics of the battery

2.2.10 Receiver and transmitter

Nowadays the most used system to establish a communication with the vehicle is the radio control. Its great advantage is its continuous updates thanks to the expansion of the aeromodelism world. However, its usage encounters a main limitation due to the fact that more than one user could be using the same frequency. Despite the possible appearance of interferences, it is decided to choose a system based on radio control because the vehicle will be flying alone over a territory.

In order to choose a model and consequently a manufacturer, the number of channels needs to be taken into account. Each channel allows one individual action to happen and four is the minimum number for quadcopters, i.e. one for throttle, one for turning right and left, one for pitching forward and backward and one for rolling left and right. Since four channels is the minimum for quadcopters and in the future extra sensors may be added to the vehicle, it is decided to choose a 6-channel transmitter.

Receivers and transmitters are not required to be from the same manufacturer as they come with a binding mechanism that allows the communication with each other. Despite this, it is preferred that both come from the same fabricator to avoid future problems.



Figure 2.2.8: Receiver and transmitter of the quadcopter

Chapter 3

Assembly and installation

In this long chapter the whole process of building the quadcopter will be gone through. For that instance the parts that came within the kit will be used along with a few additional components that were not part of it. Since no information or assembly guide was provided with the pack, a whole set of written instructions along with figures has been written to allow a future student to continue this work[5].

In order to make this process more understandable it will be split in two sections: at the hardware part and at the software level.

3.1 Hardware

First of all, it is highly recommended to cross-check all the material in the kit against the table below and contact the seller in case anything is missing. All the pack contents can be found in Table 3.1.

Quantity	Pieces
1	Upper frame plate
1	Lower frame plate
2	Red outrigger arms
2	White outrigger arms
24	M2,5*6 Mounting screws
16	M3*8 Mounting screws
1	ArduPilot Mega
4	2212 900Kv Brushless motors
4	3S 30A Brushless ESCs
2	11inc propellers (ccw)
2	11inc propellers (cw)
1	6channels radio with receiver
1	3S 1300-2600mAh LiPo battery
1	AC/DC balance charger

Table 3.1: Kit components

3.1.1 ESC's and battery soldering

First of all, two wires will be soldered to the lower board. On one hand, the two wires have a connector to hook them with the battery and on the other hand the board has an electrical printed circuit beneath its coating which is in charge of distributing the power to all the pieces soldered to it.

Secondly, the ESC's will be soldered to the board by following the same steps. It is highly advisable to check whether they work properly before soldering them together. The process to do so consists in giving power to the board and measuring their voltage.

The list of soldering-steps to follow is presented below:

1. Gather together the ESC's, the connectors, the lower board and the soldering supplies.
2. Use wire strippers to remove the insulation from each wire and expose about half centimeter of the cable at its tip.
3. Drench both the connector at the board and the tip of the wire in soldering acid.
4. Melt a drop of tinwith the soldering pencil and drop it onto the wires' tip.
5. Place the red wire in the +connector and cover the ensemble with melted tin with the help of the pencil.
6. Re-do step 5 for the black wire and the -connector.
7. Check the soldering's consistency by holding the whole assembly by the each of the pieces.

By the end of this process, the whole assembly should look the same as Figure 3.1.1 .

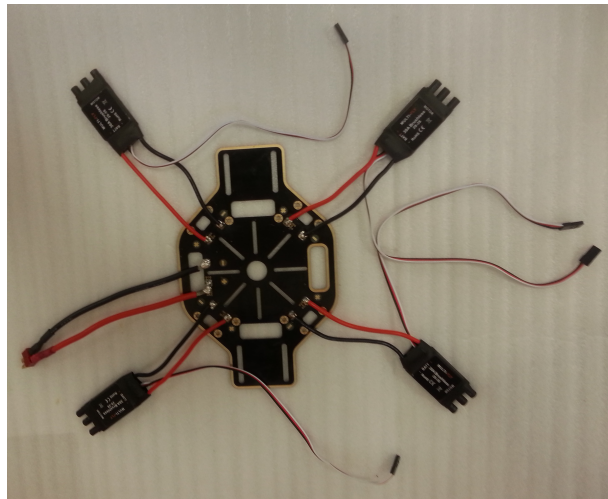


Figure 3.1.1: Battery , battery and lower frame board soldering

3.1.2 Arm assembly

Each arm has four screws in their lower surface. By using an Allen wrench, screw them to the lower board. See Figure 3.1.2 to check how the vehicle should look after this step.

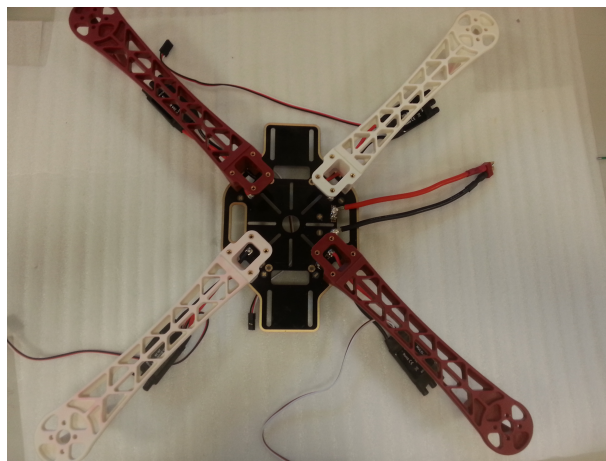


Figure 3.1.2: Arms screwed to the lower frame board

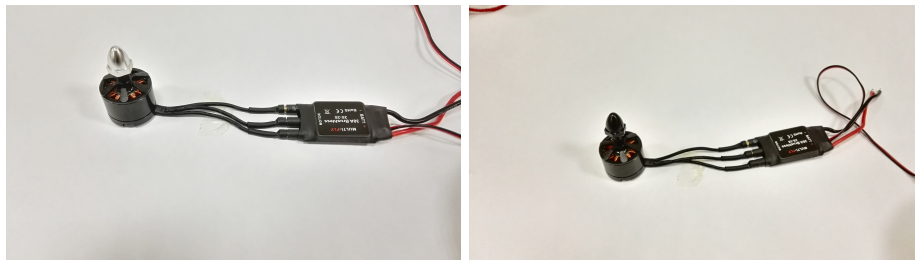
3.1.3 Motor mount-assembly

As it can be seen from Figure 3.1.3.a the motors show four holes in their inferior surface and have three small wires. On one hand, the holes are used to screw them to the arms of the structure. On the other hand the three wires determine the turning sense, i.e. clockwise or counterclockwise. Refer to the following steps to set them up:

1. Screw each motor with the help of an Allen wrench to its corresponding arm. Since this part of the vehicle is going to be exposed to higher stress than the rest of the structure, it is advisable to apply Loctite to the motor screws to prevent them from becoming loose during flight and causing a main failure.
2. In order to prevent the vehicle from spinning around itself two opposite rotors spin in one direction and the other two spin in the opposite direction so that the angular acceleration about the yaw axis is zero. In Figure 3.1.5 it can be seen how to ESCs should be connected to obtain counterclockwise [Figure 3.1.5.a] and clockwise rotations[Figure 3.1.5.b].
3. Secure the cables by putting plastic clamps around them and the arms.



Figure 3.1.3: Motor-back view



(a) Counterclockwise rotation

(b) Clockwise rotation

Figure 3.1.4: ESC's and motor wiring

3.1.4 Blades selection and assembly

As mentioned above, two rotors spin clockwise and the other two spin counterclockwise. For that instance, the blades need to have the corresponding shape. In Figure 3.1.6 it can be seen the two different forms. The steps to assemble them together are as follows:

1. Unscrew the upper bolt of the motors.
2. Insert each blade accounting for the turning sense.
3. Screw tightly the bolt using a wrench. Take into account that plastic blades are easily broken and need to be replaced, hence do not use Loctite.



(a) Counterclockwise rotation

(b) Clockwise rotation

Figure 3.1.5: Blades configuration

3.1.5 Upper board assembly

The upper board counts with sixteen holes to which the arms have to be screwed. Due to the small tolerances it is advisable to softly screw one of each arm first to adjust the board and then the rest.

3.1.6 GPS, receiver and APM assembly

These parts are attached to the upper board with the aid of plastic clamps. Moreover, since vibrations are detrimental to the electronic parts of the vehicle, soft foam-based cushions have

been prepared to act as dampers. These cushions are placed in between the GPS, APM, receiver and the board. See Figure 3.1.7 for a visual reference.



Figure 3.1.6: Damping cushions

3.1.7 Vehicle's wiring

Wiring can be said to be the most important task within the vehicle's set up, an error when connecting the cables can lead to a serious malfunction. Considering that the motors and speed controllers have already been connected (*Sub-Section 3.1.3*) the remaining wiring process will only include the APM and will be split in three stages: APM and GPS, APM and ESCs, APM and receiver.

- *APM and GPS*: the GPS cable is divided at the end in two wires and each of them is connected to the APM. The smallest end to the GPS sign on the board and the largest one to the larger pin on the same side of the board. The Figure 3.1.8 shows a diagram of the wiring for visual aid.



Figure 3.1.7: GPS wiring

- *APM and receiver*: the number of wires depends on the receiver characteristics, in this case six accounting for the number of channels plus two for transmitting the voltage. Female-female electronic wires are used to connect these two devices through the input pins on the board as follows:
 1. Pins 1 to 6 of the first row of pins the receiver are connected sequentially to the APM's first row ones.

2. Pins 7 of the receiver's second and third rows are connected to their similar pins on the APM.

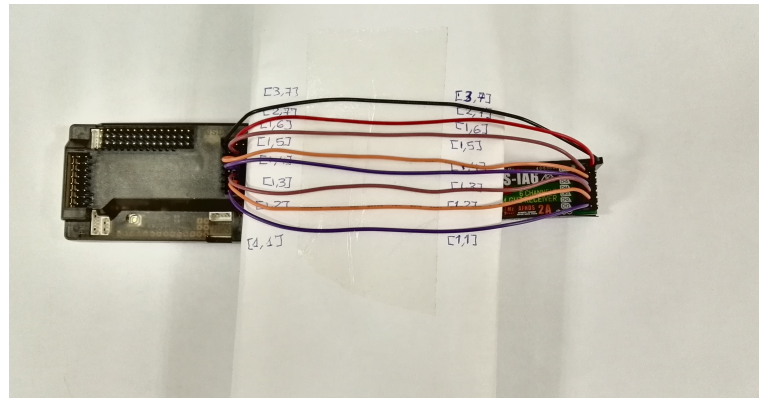
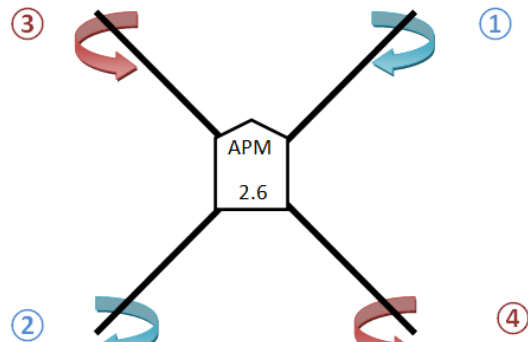


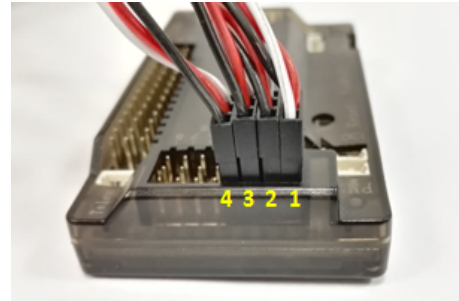
Figure 3.1.8: Receiver wiring

- *APM and ESCs*¹: the sense of rotation keeps playing an important role as it determines the order of connection between these two devices. It is highly recommended to number the motors as indicated in Figure 3.1.10 to keep track of their rotations. The connection is carried out through the output pins of the APM as follows:

1. Counterclockwise rotors are connected to the APM's output pins 1 and 2.
 2. Clockwise rotors are wired to pins 3 and 4.



(a) Motor numeration



(b) ESCs connection

Figure 3.1.9: ESCs wiring

¹ www.copter/escs/motors



25

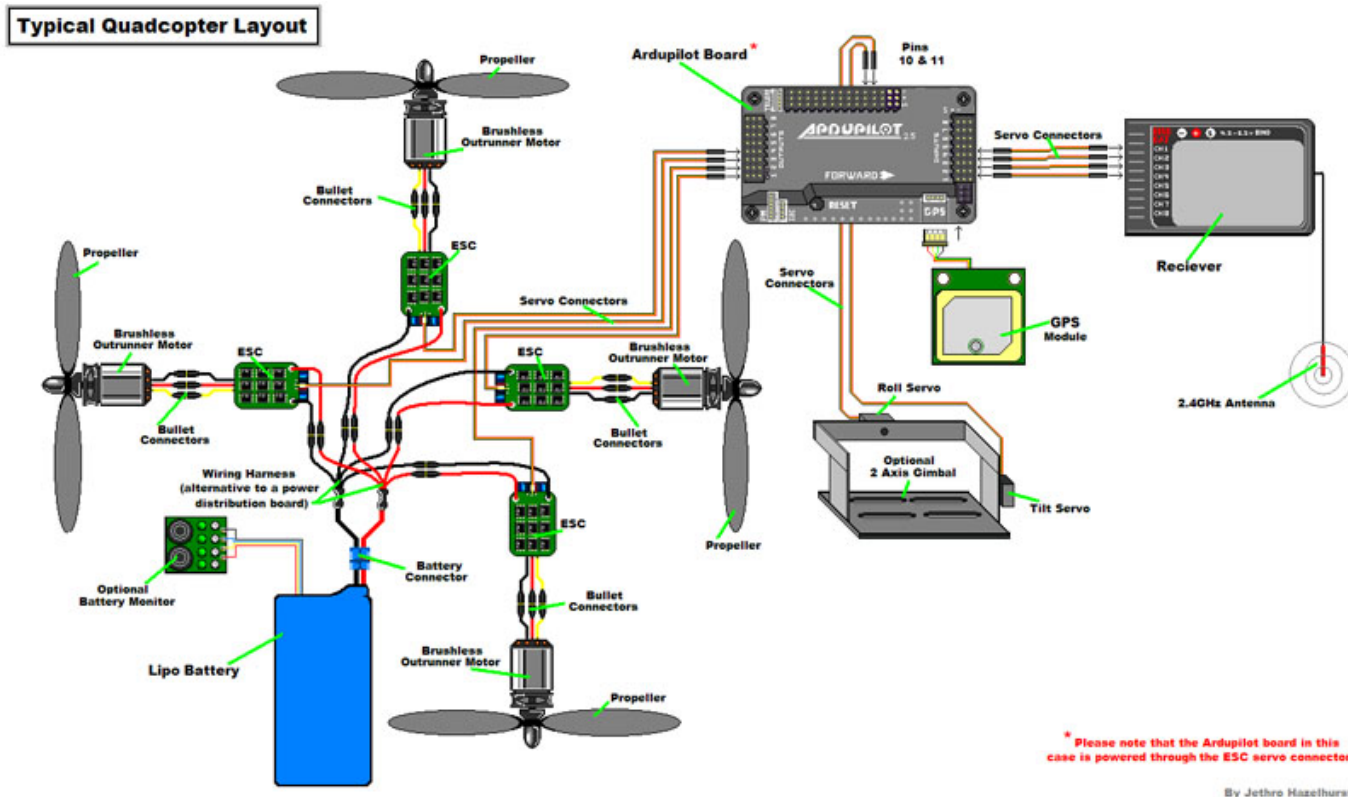


Figure 3.1.10: Vehicle's wiring © Jethro Hazelhurst / DIYDRONES



3.2 Software

At the software level, the installation and fine tuning are carried out by using Mission Planner, only compatible with Windows, or APM planner. Both applications are meant to perform equally; nevertheless their usage has proven this wrong and depending on the task to be accomplished one or the other one will be preferred. Accordingly to the project they are free, open-source and community supported applications. Moreover, they can also be used as a configuration tool or as a dynamic control supplement for the vehicle. Furthermore, these applications are provided with a friendly user interface along with a PC compatible flight simulator for UAV hardware.

This process is subdivided in two, in the first one, the drone will not be connected to computer and will allow the computer's configuration and in the second one the vehicle will be connected through an USB-miniUSB cable and the main data will be burnt onto the APM.

3.2.1 Computer preparation

First of all, the corresponding firmware for the vehicle type has to be installed in the application. In this case it would be ArduCopter v3.2.1 Quad, nevertheless, this option has been unlisted and ArduCopter v3.2.1 Hexa is automatically downloaded and established. This will be corrected when connecting the drone.

3.2.2 UAV's configuration

After connecting the vehicle to the computer it is noticeable that the applications are easy to use as they offer a wizard with all the basic hardware configuration milestones².

- *Selection of the vehicle type:* despite Mission Planner's simplicity, it is a powerful tool that allows four types of Arduino based vehicles to be configured: plane, rover, copter and helicopter. Before continuing multicopter is to be chosen.



Figure 3.2.1: Vehicle type selection

²www.nus.sg/missionplanner



- *Selection of the frame type:* even though the hexa firmware was loaded into the computer it can be fixed by selecting the X-quadcopter configuration among the seven options that are presented. This selection is loaded into the board.

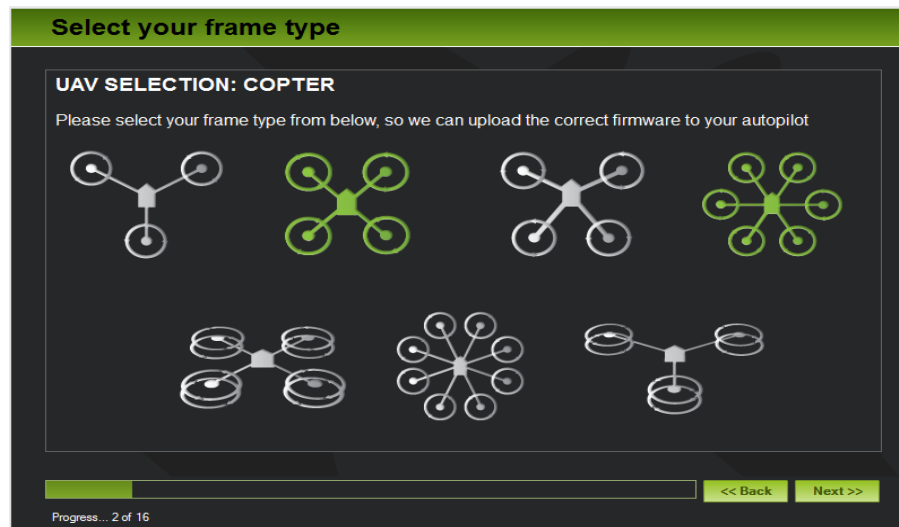


Figure 3.2.2: Frame type selection

- *Selection of the COM port:* if the port did not appear as Arduino Mega 2500 it would be required an extra configuration of the USB ports of the computer through the control panel.

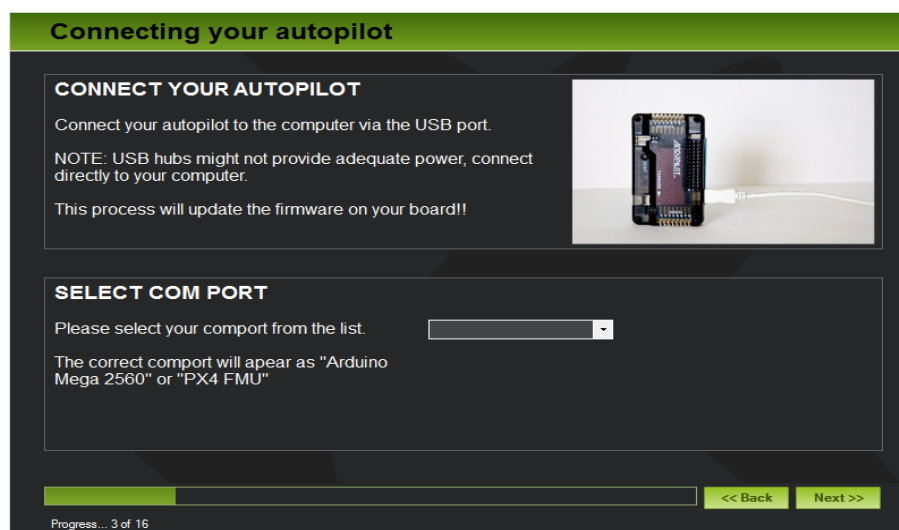


Figure 3.2.3: COM port selection

- *Calibration of the accelerometer:* this configuration needs to be carried out carefully because an unsuitable one could lead to a disorientation of the drone. For that instance, rotate the vehicle full 360 degrees aiming at the white dots. It has been observed that sometimes when using Mission Planner this configuration does not work properly, if this would happen it is recommended to switch to APM Planner, once the wizard has successfully finished, and reconfigure it.

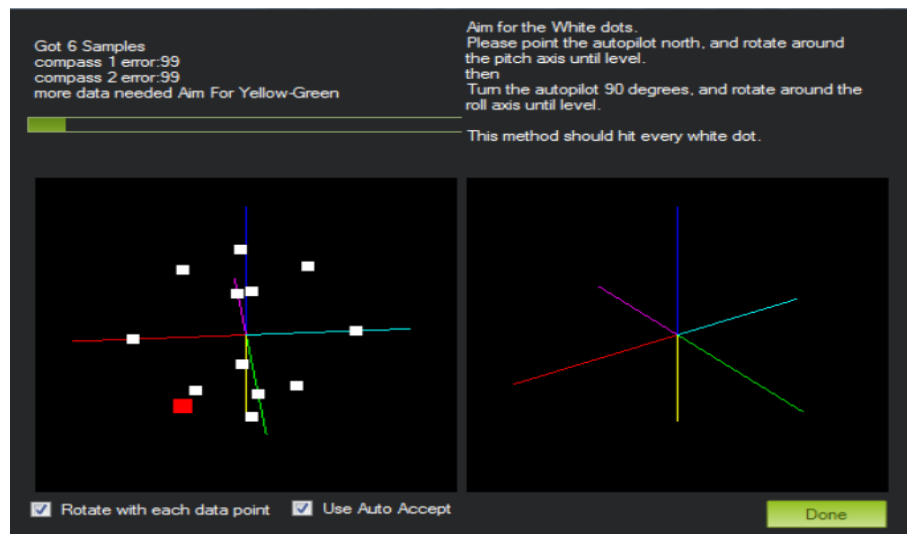


Figure 3.2.4: Accelerometer calibration

- *Configuration of the battery monitor:* the only parameter that needs to be set is the size of battery, 2600 mAh.

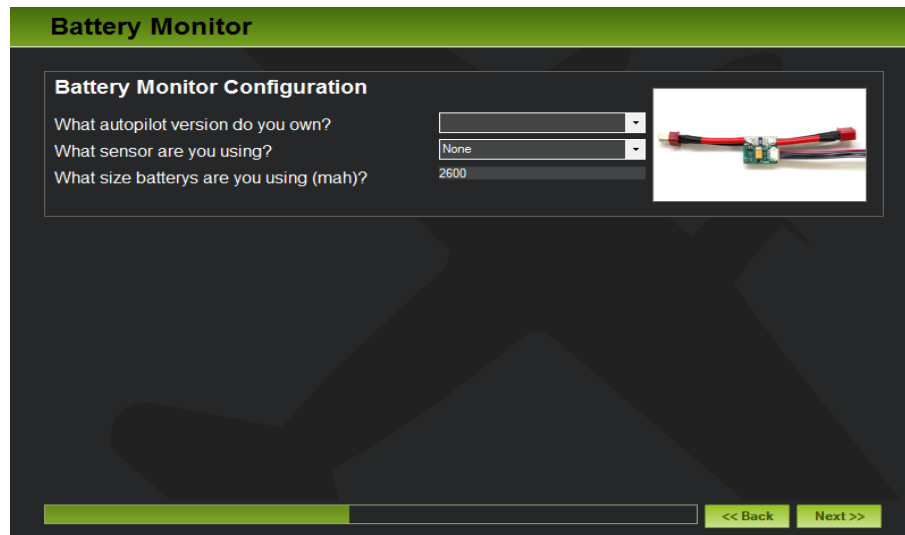


Figure 3.2.5: Battery configuration

- *Calibration of the radio:* firstly, the transmitter is switched on and once it is checked that the receiver is properly working, all the sticks need to be moved to their outer positions so the maximum and minimum values are recorded to the APM board.

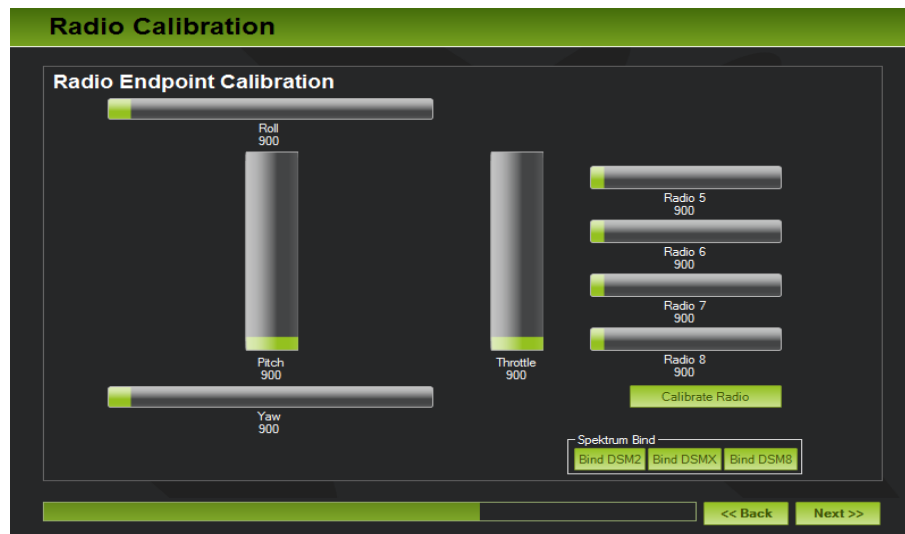


Figure 3.2.6: Radio calibration

- *Selection of the flight modes:* since a fine tuning will be later performed it is advisable to set at least two modes to stabilize and loiter.



Figure 3.2.7: Flight modes selection

Configuring through the wizard is not enough and further actions are necessary in order to have the drone fully operative:

- *Compass/motor calibration*: this step can be found under optional hardware and consists on raising the vehicle's throttle to its maximum to allow it to obtain the regular interference values that it will encounter in the work environment.
- *Calibration of ESCs*³ : sometimes new ESCs may not be calibrated. For that instance, firstly it is required to disconnect the battery and raise the throttle stick of the transmitter to the maximum. Secondly, the battery is connected and the autopilot should light up in a red, blue and yellow cyclical pattern. Thirdly, the battery is disconnected and reconnected with the throttle stick still at its maximum value, a musical tone followed by additional two beeps should be heard. This indicated that the maximum throttle has been captured. Finally, the throttle stick is pulled down to its minimum value. If a long tone was heard it would indicate that the speed controllers are calibrated, otherwise the process would need to be repeated.
- *Motor test*: it is also found under optional hardware and by selecting a throttle of at least 10% during 5 seconds an order will be sent to the corresponding motors to rotate. Moreover, this rotation will indicate whether they spin according to both sense and number.

³www.copter.com/escs

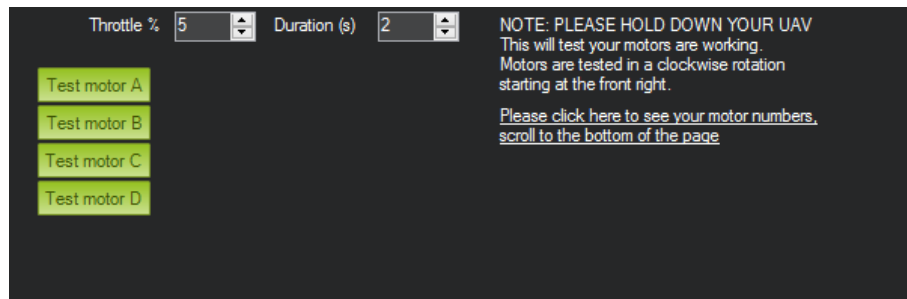


Figure 3.2.8: Mission Planner motor interface

3.2.3 Configuration of the PIDs

PIDs are three term control loop feedback mechanisms that calculate the error value as the difference between a measured process variable and a desired setpoint. To achieve this optimal result, the error is minimized by adjusting a variable. Open source quadcopters have the advantage of allowing users to change the PID configuration values to adjust the performance of their vehicles. Generally there are three PID loops with their own proportional, integrator and derivator coefficients per axis (pitch, roll and yaw) and each of them affect very differently the vehicle's behavior:

1. *Proportional gain coefficient*: this parameter is in charge of making the quadcopter fly relatively stable and determining the values measured by the gyroscopes. When changing dramatically its value it can be seen that the lower it is, the harder it is to keep the drone steady; and the higher it is, the more sensitive it is to angular variations.
2. *Integral gain coefficient*: by varying it the precision of the angular position can be increased and its usage is vital when flying with irregular cross-wind or with ground effect. However, a very low value lead to an uncontrollable oscillation and a very high value could make the quadcopter have a slow reaction.
3. *Derivative gain coefficient*: this value is key in allowing the vehicle to reach the desired attitude. It has to be taken into account that it amplifies the user's input according to its value.

The reason why the coefficients were written above in that order is because it is the one at which the drone is tuned. The process of fine tuning the vehicle is said to be trial and error as every value is changed at a time and the response of the vehicle is analyzed in order to check if it is appropriate or needs a redefinition. Furthermore, since the vehicle is symmetric it is possible to set the same values for pitch and roll. In the diagram below, the cycle to tune the quadcopter can be found:

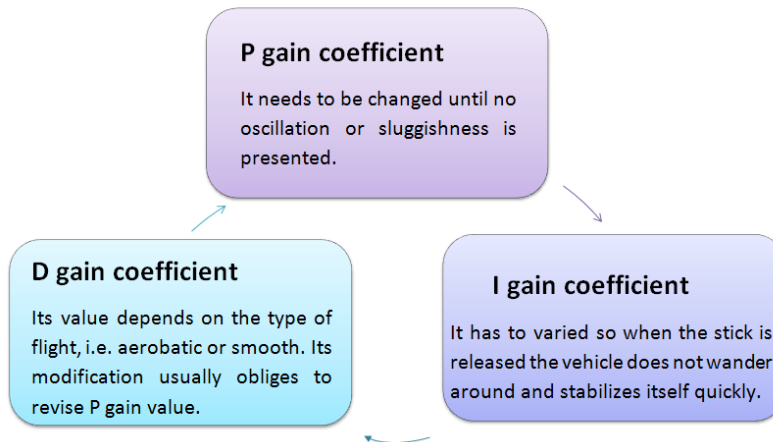
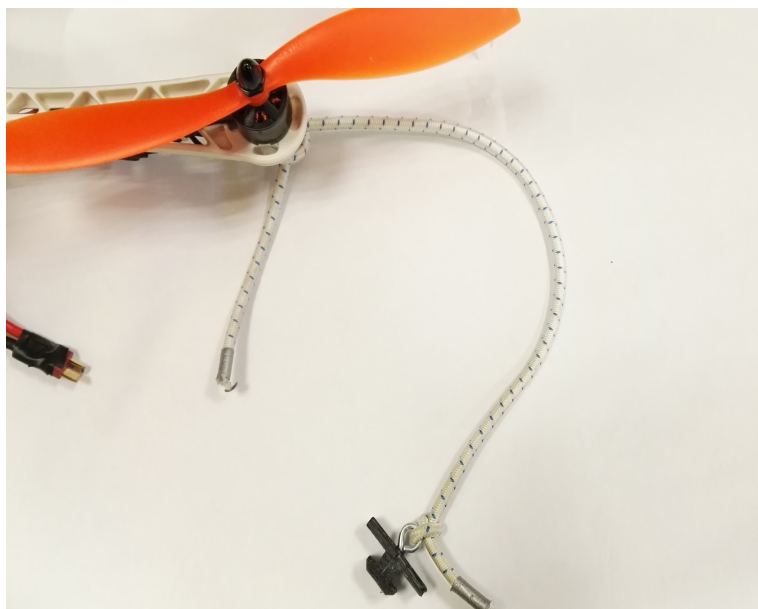


Figure 3.2.9: Quadcopter PID tuning loop

In order to start the tuning process, the vehicle is attached to a metallic structure by means of ropes and sliding rods which allow it to climb. Furthermore a foam base is placed underneath the structure to prevent it from being damaged.



(a) Metallic support and protective foam



(b) Rope with sliding rods

Figure 3.2.10: Indoor flight structure



After the completion of the tuning process⁴ the best proven values are gathered and presented in Table 3.2.

Roll	
P	0.164
I	0.05
D	0.004

(a) Roll

Pitch	
P	0.164
I	0.085
D	0.0045

(b) Pitch

Yaw	
P	0.2
I	0.002
D	0

(c) Yaw

Table 3.2: PID values

⁴www.copter.com/inflight/tuning

Chapter 4

Modeling

This chapter introduces the reader to the theoretical background behind quadcopters by going through its reference frames and equations. Furthermore, different techniques to obtain the needed parameters that will allow the simulation are presented.

4.1 Theoretical background

In order to build a model to predict the dynamics of any mechanical system, the first step is to write down its equations of motion. Since the derivation of these equations is out of the goal of this project it has only been included in Appendix A. This process is based on the work developed by [6]

4.1.1 Reference frames

It is considered that the quadcopter consists of an airframe and four blades and for simplicity it is considered that they are rigid bodies linked by ideal rigid joints. The plant of the quadcopter is simplified to a structure that consists of four blades with their corresponding arms connected to each other at the center of the vehicle. This interpretation implies the usage of three reference frames: one inertial frame, one body frame and one blade frame.

1. *Inertial frame*: it is placed in a static point on the Earth and from there the user will control the drone. This frame is denoted by the sub-index E and is defined by the unit vectors $[\mathbf{i}_E, \mathbf{j}_E, \mathbf{k}_E]$
2. *Body frame*: it is attached to the airframe at its center of masses and moves according to the vehicle's movement. It has the origin at O_B and their axes O_X and O_Y are contained in arms 1 and 2. For further details, refer to Figure 4.1.1.
3. *Blade frame*: four more non inertial frames are used to describe the propellers' motion. Each of them is attached to their corresponding blades' center of masses. In order to avoid confusion, each frame will be numerated from 1 to 4, according to the blades' number and their Y_N axis will run parallel to the blade with its center at O_N .

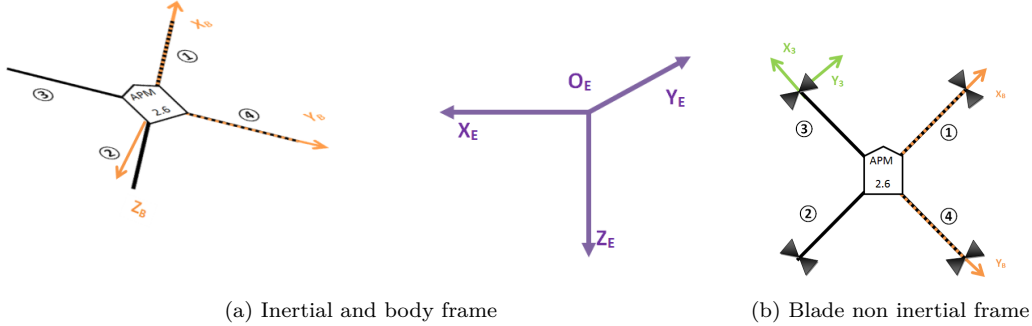


Figure 4.1.1: Frames of the vehicle

4.1.2 Equations of motion

The equations of motion are necessary to describe the behavior of the system in terms of the motion and as a function of time, more specifically in terms of spatial coordinates, Euler angles and their derivatives with respect to time. As it was expected these equations contain complex couplings that need to be simplified as much as possible to obtain a solution for the system. For that instance, simplification assumptions are made and they also comprise linearization premises to allow the implementation of a controller that will be used to eliminate the possible disturbances around the equilibrium state. Furthermore this dynamic model will lead to the obtention of the changes of the spatial coordinates and their derivatives.

The kinematic equations are expressed in the Earth fixed frame and are as follows:

$$\begin{aligned} x &= (\cos\psi\cos\theta)x + (\cos\psi\sin\theta\sin\phi - \sin\psi\cos\phi)y + (\cos\psi\sin\theta\cos\phi + \sin\psi\sin\phi)z \\ y &= (\sin\psi\cos\theta)x + (\sin\psi\sin\theta\sin\phi + \cos\psi\cos\phi)y + (\sin\psi\sin\theta\cos\phi - \cos\psi\sin\phi)z \\ z &= (-\sin\theta)x + (\cos\theta\sin\phi)y + (\cos\theta\cos\phi)z \end{aligned} \quad (4.1.1)$$

The aerodynamic forces and moments are expressed in six different contributions:

1. *Rolling moment*: it is produced by a variation of thrust in motors 1 and 2
 - (a) Body gyro effect $\dot{\theta}\dot{\psi}(I_{yy} - I_{zz})$
 - (b) Propeller gyro effect $J\dot{\theta}\Omega_r$
 - (c) Roll actuators action $bl(\Omega_3^2 - \Omega_4^2)$
where I_{yy} and I_{zz} are the moments of inertia around the y and z- axes respectively, l is the arm's longitude and Ω_3 and Ω_4 are the thrust of motors 3 and 4 respectively.
2. *Pitching moment*: it is produced by a change of thrust of motors 3 and 4 (Fig 4.6.1.b):
 - (a) Body gyro effect $\dot{\theta}\dot{\psi}(I_{zz} - I_{xx})$
 - (b) Propeller gyro effect $J\dot{\phi}\Omega_r$
 - (c) Roll actuators action $bl(\Omega_2^2 - \Omega_1^2)$
where I_{xx} is the moment of inertia around the x axis and Ω_1 and Ω_2 are the thrust of motors 1 and 3 respectively.

3. *Yawing moment*: the thrust of the clockwise motors is increased the same value and the one of the counterclockwise one decreased or viceversa.

- (a) *Body gyro effect* $\dot{\theta}\dot{\psi}(I_{xx} - I_{yy})$
- (b) *Counter-torque unbalance*: it is caused by the drag moment acting on the blades.
 $-Q_1 - Q_2 + Q_3 + Q_4$
 where $Jr = 2/3mR^2$, R is the radius of the blade , $Q_i = 1/2C_D\rho AR^3\Omega_i^2$, A is the cross section of the blade and Ω_i the angular velocity of each blade.

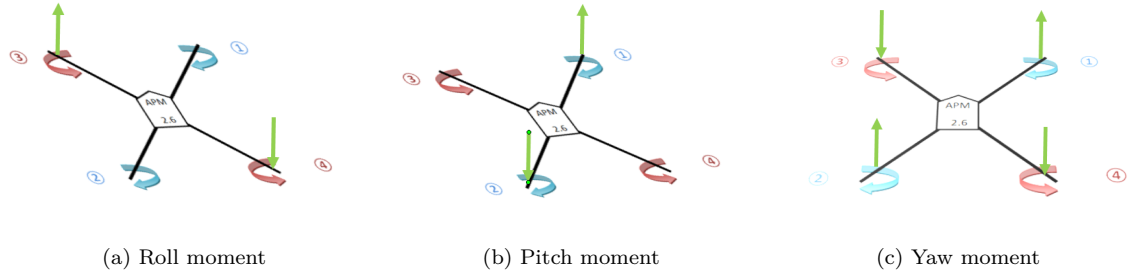


Figure 4.1.2: Aerodynamic moments

4. Forces along x-axis:

- (a) Actuators action $(\sin\psi\sin\phi + \cos\psi\sin\theta\cos\phi)(\sum_{i=1}^4 b\Omega_i)$
- (b) Friction $\frac{1}{2}C_x A\rho x |\dot{x}|$

5. Forces along y-axis

- (a) Actuators action $(-\cos\psi\sin\phi + \sin\psi\sin\theta\cos\phi)(\sum_{i=1}^4 b\Omega_i)$
- (b) Friction $\frac{1}{2}C_y A\rho y |\dot{y}|$

6. Forces along z-axis:

- (a) Actuators action $\cos\psi\cos\phi(\sum_{i=1}^4 b\Omega_i)$
- (b) Weight mg

Gathering all the equations together the following set is obtained:

$$I_{xx}\ddot{\phi} = \dot{\theta}\dot{\psi}(I_{yy} - I_{zz}) + l(\Omega_3 - \Omega_4)$$

$$I_{yy}\ddot{\theta} = \dot{\theta}\dot{\psi}(I_{zz} - I_{xx}) + l(\Omega_1 - \Omega_2)$$

$$I\ddot{\psi} = \dot{\theta}\dot{\psi}(I_{xx} - I_{yy}) + J_r\dot{\Omega}_r - Q_1 - Q_2 + Q_3 + Q_4$$



(4.1.2)

$$\begin{aligned} m\ddot{z} &= mg - (\cos\psi \cos\phi) \sum_{i=1}^4 b\Omega_i \\ m\ddot{x} &= (\sin\psi \sin\phi + \cos\psi \sin\theta \cos\phi) \sum_{i=1}^4 b\Omega_i \\ m\ddot{y} &= (-\cos\psi \sin\phi + \sin\psi \sin\theta \cos\phi) \sum_{i=1}^4 b\Omega_i \end{aligned}$$

where C_x and C_y are the drag coefficients in the x and y axes respectively and $b = \pi C_T \rho R^4 / m_q l$

4.2 Estimation of drag and thrust coefficients

As it can be seen from the previous pages, almost all the equations depend on both the drag and the thrust coefficients. Hence, the obtention of these dimensionless parameters is key in order to fully describe the UAV's motion. The way in which both drag and thrust appear is as follows: The application of momentum theory to the blades results in the thrust. At the same a reactive torque due to the aerodynamic drag appears over each blade. This torque needs to be compensate by the electrical motors to keep the blade spinning. In order to see the dependencies of these two parameters their equations are presented below:

$$M_j = C_D \rho A \Omega^2 \frac{1}{2} \quad (4.2.1)$$

$$T_j = C_T \rho \pi R^4 \Omega^2 \quad (4.2.2)$$

Where Ω is the angular velocity of the blade, R the radius of the blade, T_j the thrust, M_j the torque produced by the motors and A the cross section of the blade.

4.3 Test bench setup

In order to obtain these two parameters, the thrust force needs to be computed. For that instance the motor is firmly mounted onto a scale which is capable of measuring down to half grams. It also has the capability of measuring negative forces, which means that if the scale's plate is lifted it will displayed a negative weight. Thus, it will be assumed that the thrust force equals the weight displayed by the scale. Another important issue when trying to be as accurate as possible is avoiding the ground effect. According to theory of helicopters, to avoid this effect, a distance between the blade and the ground of at least the length of the blade is necessary. As a consequence, a wooden support is constructed. This structure will be mounted onto the scale and the motor will be taped to it. Figure 4.3.1.a below shows the whole structure

Once the whole structure is assembled, the throttle is carefully risen. Each time it is incremented, the voltage and current of the motors, weight displayed on the scale and the angular velocity of the blade are measured. In order to acquire the angular velocity a tachometer is used. This device works by emitting a red ray and by counting the times that the beam is interrupted

by a rotating reflective object. For that purpose, a strip of a reflective paper is taped to half of the propeller.



(a) Test bench setup



(b) Reflective paper taped to propeller

Figure 4.3.1: Test bench setup

4.4 Test bench results

After the needed data is acquired, it is gathered in Appendix B to ease its representation.

On one hand, , since according to Equation 4.4.1 the motor produces a torque to overcome the aerodynamic drag force, it is stated that the power that inputs the motor equals the voltage multiplied by the current. Therefore the torque that is created will be equal to the power that exits the motor divided by the angular velocity. Both powers are related by the motor's efficiency.

$$M_j = \frac{P_{OUT}}{\Omega} = \frac{P_{IN}\eta}{\Omega} = \frac{V * I * \eta}{\Omega} \quad (4.4.1)$$

By plotting M_j against Ω^2 and after linearly approximating it, the slope of the graph is found. By diving this value by $\rho AR/2$ the drag coefficient is found.

One the other hand, according to Equation 4.2.2 the weight (T_j) is plotted against Ω^2 to obtain by a linear approximation made by Excel the slope. To obtain the thrust coefficient this slope is divided by $\rho\pi R^4$.

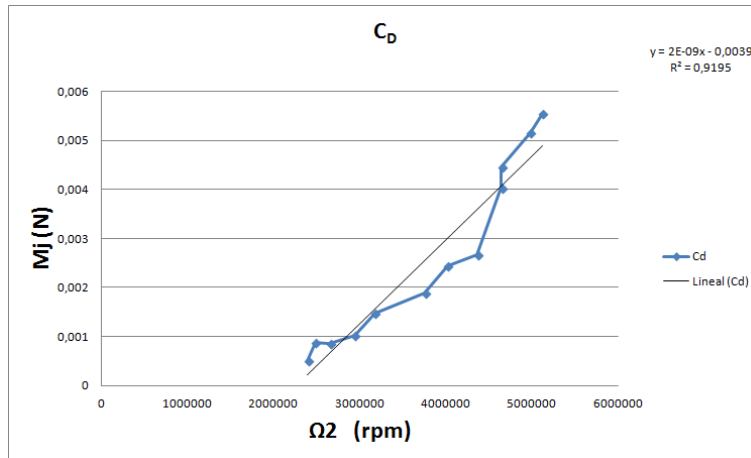


Figure 4.4.1: Momentum (M_j) vs. Ω^2

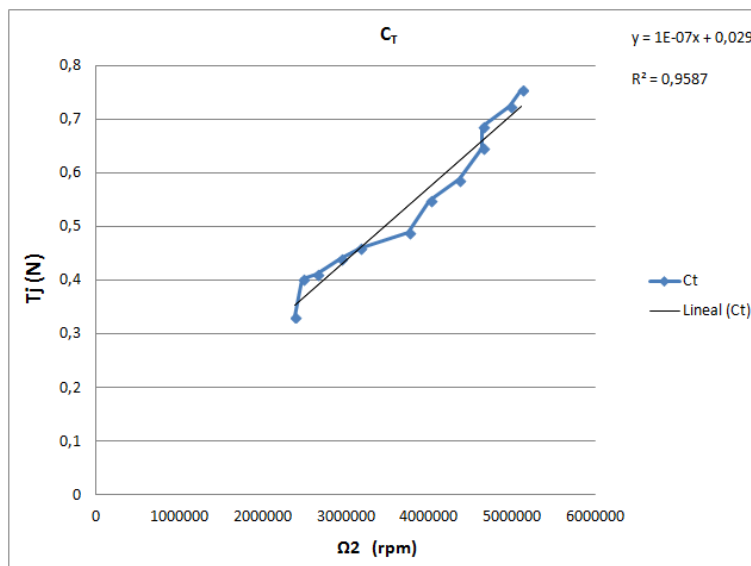


Figure 4.4.2: Thrust (T_j) vs. Ω^2

Due to the short number of decimal numbers that Excel works with this very same process is manually repeated. For this purpose, a table for each subsection is constructed and by applying Equation 4.4.2 and Equation 4.4.3 the slopes are found. Finally by dividing these values by the above mentioned parameters, both drag and thrust coefficients are obtained.



$$m = \frac{n \sum_{i=1}^n x_i y_i - \sum_{i=1}^n x_i \sum_{i=1}^n y_i}{n \sum_{i=1}^n x_i^2 - \left(\sum_{i=1}^n x_i \right)^2} \quad (4.4.2)$$

$$b = \frac{\sum_{i=1}^n x_i^2 \sum_{i=1}^n y_i - \sum_{i=1}^n x_i \sum_{i=1}^n x_i y_i}{n \sum_{i=1}^n x_i^2 - \left(\sum_{i=1}^n x_i \right)^2} \quad (4.4.3)$$

Where m is the slope of the graph and b is the intercept.

The values of the drag coefficient and the thrust are found in Table 4.1.

m	$1,71363 * 10^{-9}$
b	$3,866275 * 10^{-3}$
C_D	$3,41347 * 10^{-5}$

(a) Drag

m	$1,35949 * 10^{-7}$
b	$2,299292 * 10^{-2}$
C_T	$2,708042 * 10^{-3}$

(b) Thrust

Table 4.1: Graphs parameters

4.5 Estimation of mass and inertial properties

To successfully build a model of the flight dynamics of the quadrotor it is essential to know its mass and inertial properties. It was previously seen that the following information from each of the moving parts, blades and airframe, is needed:

- Mass
- Coordinates of the center of mass
- Moments and products of inertia

It is evident that the more accurate these results are , the better the simulation will be.

4.5.1 Use of commercially available CAD tool

As for obtaining the masses, the vehicle is disassembled and every component is weighted. Even though it could be thought that only two values were needed: blades and airframe, all the masses are needed to obtain the moments of inertia.

Obtaining the position of the center of mass and the values of moments of inertia is not as easy as the masses. There are two possible approaches, theoretically and experimental. If properly carried out, the second approach is preferable as it outcomes the results of the real quadcopter not of an approximation to it. However, the computations to attain these values on the real scale vehicle can be very complicated and might not be cost effective. Thus the theoretical approach is chosen.

Once it is decided to leave the experimental approach aside, the most effective way to proceed is by using one of the many softwares that CAD has available[7]. In this case SolidEdge ST7 is used to model each component of the vehicle to allow the obtention of their inertia. This program is also capable of computing the volume the center of mass, the moments, products of inertia and the principal moments of inertia of any drawing. For that instance, every component is measured, drawn at full scale in SolidEdge and their masses are introduced. The reason why the mass assignation process is carried out for every component before assembling them together is because all the parts are made of different materials with very different mass properties. The mass values can be found in Appendix C.

Moments of inertia	Value ($g.cm^2$)
I_{xx}	142014,03
I_{yy}	194685,94
I_{zz}	137220,55
$I_{xy} = I_{yx}$	-436,61
$I_{xz} = I_{zx}$	-344,41
$I_{yz} = I_{Izy}$	-1793,95

Table 4.2: Moments of inertia obtained from CAD drawing

An image of the model of the vehicle is shown below. Moreover, the plans of every component along with their dimensions can be seen in Appendix D.

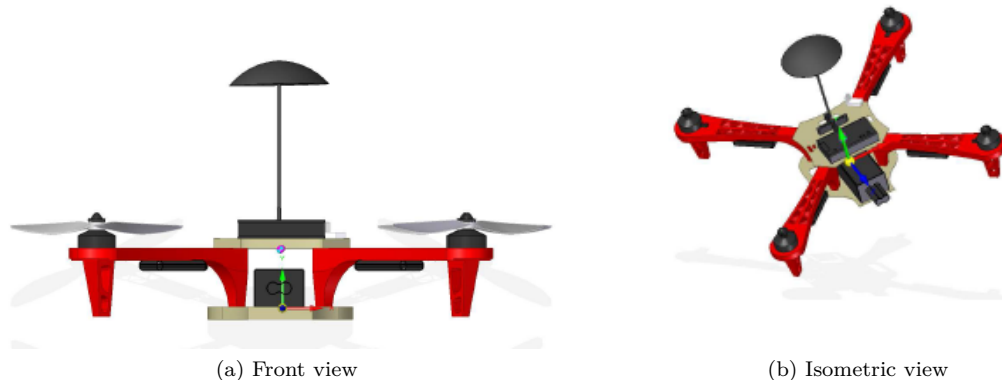


Figure 4.5.1: SolidEdge drone model

It should be mentioned that the SolidEdge model is not completely detailed. Some parts such as the motors have a simplified geometry as it is not advisable to disassemble them. Moreover, wiring has not been included either.

Chapter 5

Simulink modeling

With the rapid development of high speed computers during the recent decades, a new approach to control system designs has been created. In this theory, the control system is specified as a system of first-order differential equation. By formulating the problem in this manner, the control system designer can fully exploit the digital computer for solving complex control problems. Within this rapid development of control theory, new demands have been created and programs such Matlab/Simulink have emerged to satisfy them.

5.1 State space modeling

In the first approach it is considered the idea of reducing Equations 5.1.1 to a set of first order linearized equations in order to express them as a state-space system [8].

$$\dot{x} = Ax + B\eta \quad (5.1.1)$$

where \dot{x} is the input vector, x the state vector, η the control or input vector ,A the plant matrix and B the control matrix.

By substituting all the parameters by the sum of themselves and a disturbance and linearizing the resulting equations are as follows:



$$\begin{aligned}
x_1 &= \phi \\
x_2 &= \dot{x}_1 \\
x_3 &= \theta \\
x_4 &= \dot{x}_3 \\
x_5 &= \psi \\
x_6 &= \dot{x}_5 \\
x_7 &= z \\
x_8 &= \dot{x}_7 \\
x_9 &= x \\
x_{10} &= \dot{x}_9 \\
x_{11} &= y \\
x_{12} &= \dot{x}_{11}
\end{aligned} \tag{5.1.2}$$

$$\begin{aligned}
\dot{x}_1 &= x_2 \\
\dot{x}_2 &= x_4 x_6 \frac{I_{yy} - I_{zz}}{I_{xx}} + x_4 \frac{J_r}{I_{xx}} \Omega_r + \frac{l}{I_{xx}} \\
\dot{x}_3 &= x_4 \\
\dot{x}_4 &= x_4 x_6 \frac{I_{zz} - I_{xx}}{I_{yy}} - x_4 \frac{J_r}{I_{yy}} \Omega_r + \frac{l}{I_{xx}} U_3 \\
\dot{x}_5 &= x_6 \\
\dot{x}_6 &= x_4 x_2 \frac{I_{xx} - I_{yy}}{I_{zz}} - \frac{1}{I_{zz}} U_4 \\
\dot{x}_7 &= x_8 \\
\dot{x}_8 &= g - \frac{1}{m} (\cos x_1 \cos x_3) U_1 \\
\dot{x}_9 &= x_{10} \\
\dot{x}_{10} &= \frac{1}{m} (\cos x_1 \sin x_3 \cos x_5 + \sin x_1 \sin x_5) U_1 \\
\dot{x}_{11} &= x_{12} \\
\dot{x}_{12} &= \frac{1}{m} (\cos x_1 \sin x_3 \sin x_5 - \sin x_1 \cos x_5) U_1
\end{aligned} \tag{5.1.3}$$

where $\begin{cases} U_1 = \Omega_3^2 + \Omega_4^2 + \Omega_1^2 + \Omega_2^2 \\ U_2 = \Omega_3^2 - \Omega_4^2 \\ U_3 = \Omega_1^2 - \Omega_2^2 \\ U_4 = \Omega_3^2 + \Omega_4^2 - \Omega_1^2 - \Omega_2^2 \end{cases}$

As it can be seen, not all the equations can be expressed in a matrix form as they still depend on more than one state. For that reason the state space modeling approach to solve the equations of motion is disregarded and the non-linearized equations will be implemented in Simulink.

5.2 Simulink model

In pursuance of obtaining the most accurate simulation it is decided to reproduce step by step the process undergone by the vehicle.

Accordingly, this procedure ranges from obtaining the different commands and deciphering the response according to them. As a result the final model is broken down in four main systems with a clearly defined function:

1. *Inputs:* There are four inputs that correspond to the real transmitter's ones: throttle, pitch, roll and yaw. These four values are created by a Simulink block called Signal Builder which allows importing time structures. In *Section 6.4* it will be seen how to export these data from the real vehicle and import them into these blocks

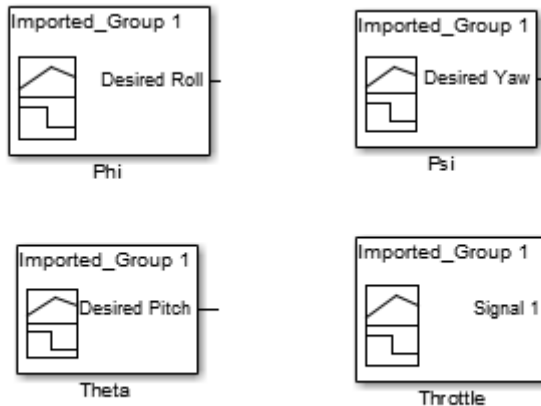


Figure 5.2.1: Simulink system inputs

2. *Conversion:* Since the throttle input is an electronic signal, a conversion needs to be found and implemented. For that reason, the relationship between the angular velocity of the blades and the throttle input is studied. It is noticed that these speeds vary proportionally to the throttle fluctuations. To that end, the test bench is set up again to measure the blades angular velocity that correspond to each input variation. Finally the relationship is inserted into Simulink.

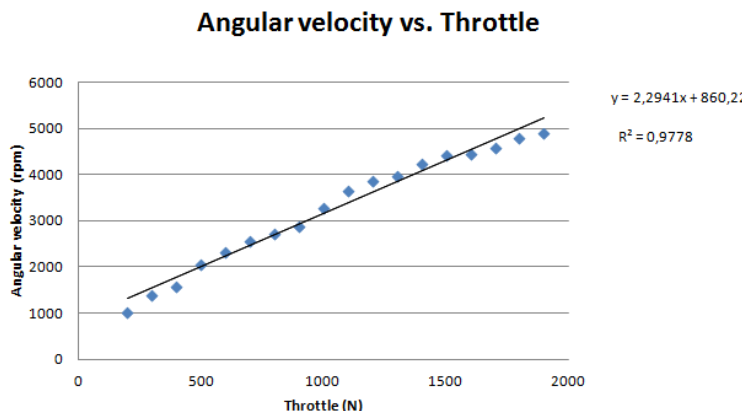


Figure 5.2.2: Variation of ω with respect to *throttle*

3. *Controller*: this block contains the PID controller developed to stabilize the vehicle. Its structure and tuning will be explained in Section 5.3.
4. *Airframe*: This subsystem is the most complex one as it computes the displacements, velocities and acceleration of the body as well as the variations of the Euler angles and angular rates. This is achieved by implementing the set of Equations 5.1.3 into Simulink.
5. *Graphs*: the relevant data is plotted and presented to the reader.

Further details of the Simulink can be found in Appendix F.

5.3 PIDs

It was previously mentioned that a system controller will be implemented to eliminate the steady error and to make the system angles be more accurate with respect to the desired ones. Before implementing the controller it is very important to understand how they will affect the output's behavior. For that reason Table 5.1 below introduces the reader to some of their effects.

Parameter	Stability	Overshoot	Settling time	Error
Proportional	DEGRADE	INCREASE	NO CHANGE	DECREASE
Integral	DEGRADE	INCREASE	INCREASE	ELIMINATES
Derivative	IMPROVE	DECREASE	DECREASE	NO CHANGE

Table 5.1: Effects of increasing each parameter

After analyzing the table, it is decided to implement the three parameters on the first instance and manually change their values until the output resembles the input within a short time. In order to implement them, there are two options, either use the PID Simulink block which integrates the three of them or model them separately. Since it is not sure that the three will be necessary to stabilize the angles ,individual controllers will be implemented according to Equation 5.3.1:

$$u(t) = K_p e(t) + K_i \int_0^t e(\tau) d\tau + K_d \frac{de}{dt} \quad (5.3.1)$$

where K_p , K_i and K_d are the proportional, integral and derivative coefficients respectively and e is the error .

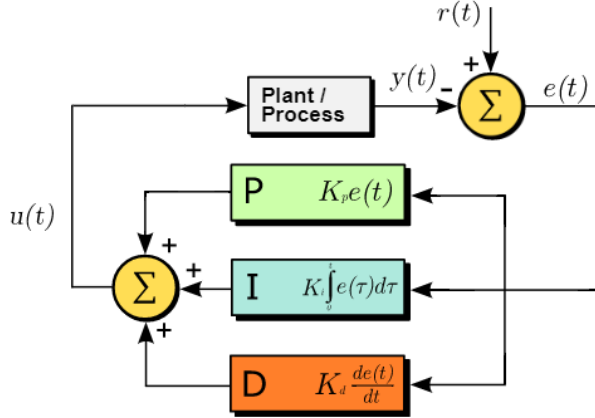


Figure 5.3.1: PID scheme

5.3.1 PID tuning

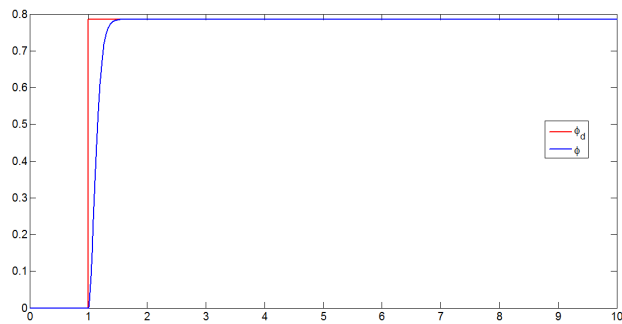
The goal of adjusting the PID parameters is to make the control loop corrects effectively and in the minimum time the disturbances errors. Adjusting a control loop implies modifying the system parameters to an optimum value. A method to adjust these parameters consist in developing a consistent methodology to choose the P I and D parameters that better stabilize the system. In this case the following steps are followed¹:

1. Set I and D to zero
2. Increment P to a value at which the output oscillates around the equilibrium position.
3. Finally set P to half of the value of step 2.
4. Raise I to a value in which the output fits in the stabilization required time. It should be noticed that a high I value could cause instability.
5. Increment D so the output is capable of adjusting itself to the desired shape when a abrupt change in its motion.

By following this methodology and repeating the steps until the output angles match the desired ones the PID values are found.

1. *Roll tuning:* the desired output is limited to 45° which is thought to be the maximum inclination angle that this vehicle will normally encounter. As it can be seen in Figure 5.3.2.a below, the angle is adjusted to the required angle within 1.47 seconds.

¹www.wikipedia.org/PID/manualtuning

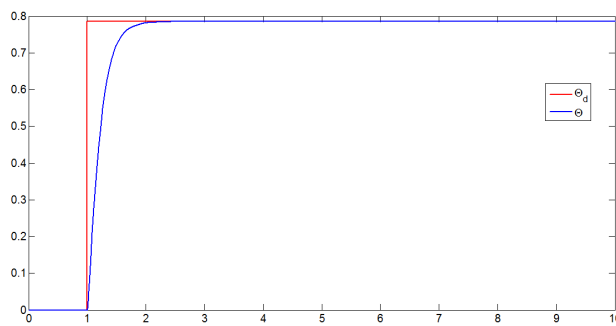
(a) Comparison ϕ and ϕ_D

ϕ	
Proportional	3
Integral	0
Derivative	0.4

(b) Roll PID values

Figure 5.3.2: Roll PID tuning

2. *Pitch tuning:* since roll and pitch in a quadcopter can be said to be equal due to its symmetry, it is also set to 45° . However, as it can be seen by comparing the charts 5.3.2.b and 5.3.3.b the stabilizing values are not the same. This is due to the fact that the inertia moments found in CAD are introduced in the dynamic model, making roll and pitch be different. Moreover, it needs to be highlighted that pitch needs 2.3 seconds.

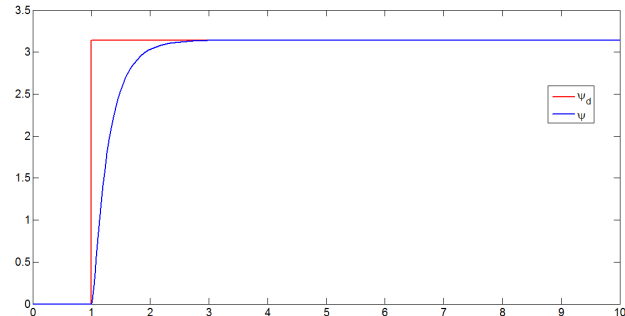
(a) Comparison θ and θ_D

θ	
Proportional	1.3
Integral	0
Derivative	0.4

(b) Pitch PID values

Figure 5.3.3: Pitch PID tuning

3. *Yaw tuning:* the desired output is set to 180° and its stabilization time is 3.25 seconds which is the highest value within the three angles. However, this value is still an optimum one.

(a) Comparison ψ and ψ_D

ψ	
Proportional	2.64
Integral	0
Derivative	0.5

(b) Yaw PID values

Figure 5.3.4: Yaw PID tuning

Chapter 6

Experimental results

This chapter aims to retrieve real flight data for later comparison in Chapter 7 with the theoretical results. In order to fulfill this objective two milestones need to be accomplished before: familiarization with the software usage and deep understanding of the vehicle capabilities.

6.1 Software familiarization

As reviewed in previous sections, this program is an user friendly interface that allows both the vehicle calibration and the reviewing of real flight data. Its initial screen shows eight different windows that allow a total management and redefinition of the vehicle's interpretation to a given command. A brief summary of the functions of the most relevant windows is presented below:

- *Flight data:* it displays a simulated horizon that enables users deduce how leveled the RPAS is. Moreover, a Google maps based plan showing the current position is visible. Its accuracy depends on the GPS used. Furthermore, the vehicle can be armed from this window, its flight logs can be reviewed and its telemetry options can be configured.

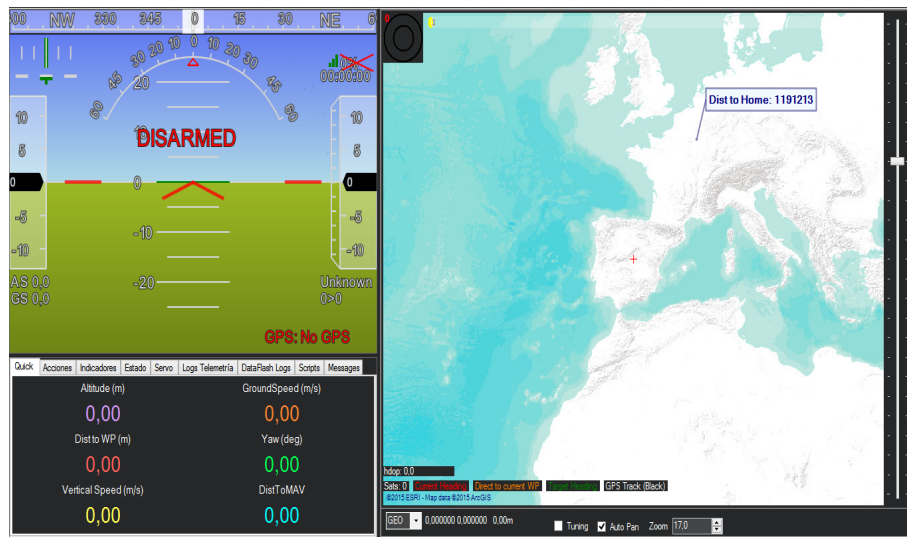


Figure 6.1.1: Mission planner Flight Data

- *Flight plan:* from this window different map views can be displayed and the desired waypoints can be loaded to the processor.

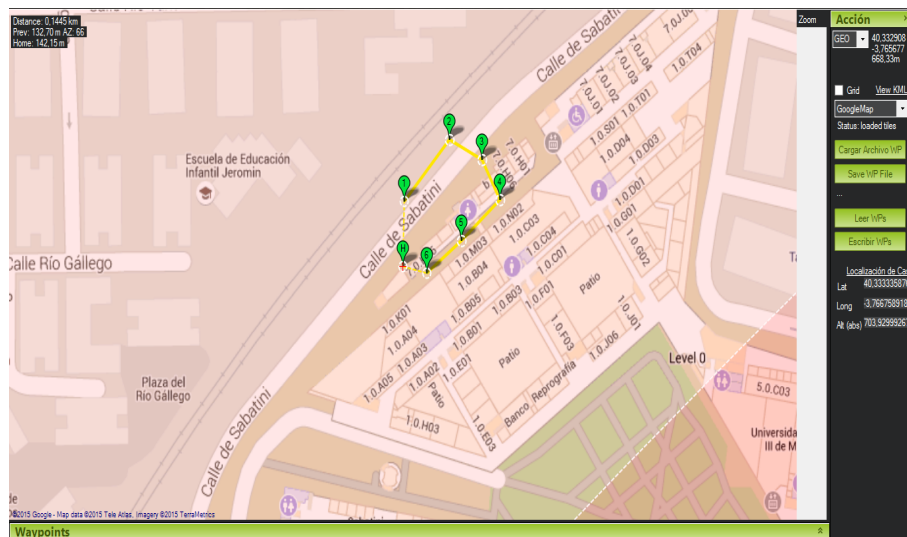


Figure 6.1.2: Mission Planner Flight Plan

- *Initial setup:* as seen in Section 3.2 this feature contains the firmware installation and the initial configuration process.



- *Configuration/Tuning:* this window is by far the most sensitive one of the program, as it contains the values of the PIDs. It is highly advisable to not change any value in here unless it is completely necessary as a minimum variation in any of the numerical values could lead to a catastrophic drone's destabilization. It is recommended to fine tune the values with the transmitter before varying them in the software.

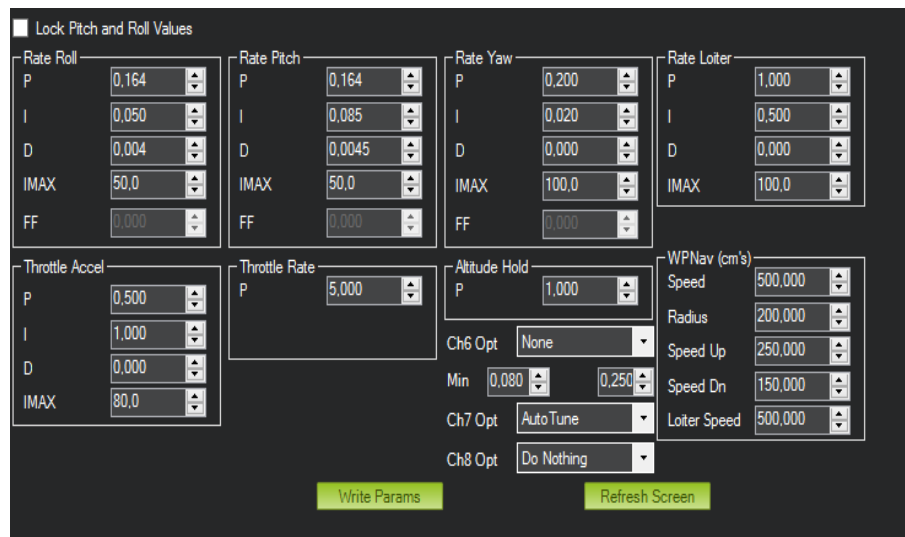


Figure 6.1.3: Mission Planner Configuration/Tuning

- *Terminal:* it lets the most advanced users access the data stored in the processor and modify it by inputting Arduino-based commands.



```

APM Connect
Show Settings Setup Radio Tests Log Download Log Browse
*NOTE* Please click connect above
CLI Works only on first connect of power, log download only over USB
Newer versions only support log download via mavlink, please see the flightdata > dataflahs logsOpened com port

Init ArduCopter V3.2.1 (36b405fb)
Free RAM: 1999
FW Ver: 120
-----
load_all took 34220us
Q?3Calibrating barometer_RQ 3 barometer calibration completeo3GROUND STARTt?Init Gyro*Q.P*
Ready to FLY <p9u>#xJd:.
@ j+1
* ubiox >7`8)c$9(#qeDtV90_JtX6$A|?<Av> `wjD (\ \
/ / EM4*1@V
9.MF9<+1k\c$SA0#+M:8T9ICpB: J==<
<>V!:==<x" # (d-x*?Q~•*+pIw )wb&wjD
92
H'/ / / F(\_) * &xx<PV
9M++<8<c\, !cUO-$I..#0/sz3+-K8790<0_0J{ .>{ .>
#GL1D=<?=<02X3K<x24+_Qv'@*5xjD (<
/ )6: / / 97m8*:98d0V
9tm:>X=r0:St3dq:$QB=#>cy=~@:O<@pL?J>>Q) \@B=Cs=@ABp~x*CQ) ?D+QYw'@!ExjDR<4
F/ / / DGm, tBn@IXW
9M'J>4-rgf!Vd2L\$ (YD7M#RN;=u-@:O<9]OJz>z>(. Q8 :P<Jo=QR.~xQS+?av* ' TNxJd:.
U/ / / LIVmEWKDX'W
9MI>Y>jz>BZ!NW

```

Figure 6.1.4: Mission Planner Terminal

6.2 Vehicle capabilities

Before diving any deeper into extracting the real flight data it is important to understand which data can be retrieved and its meaning. For that purpose, the vehicle capabilities and more specifically the processor ones need to be studied. Even though at first glance APM 2.6 may seem a small and simple device, it has some integrated systems that allow it to infer its motion and position. These entities are as listed hereinafter:

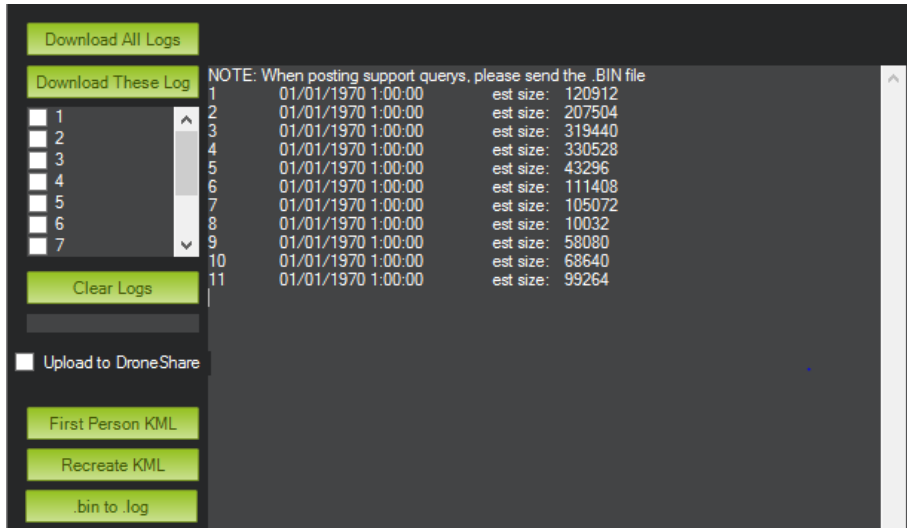
- *Gyroscope*: it helps determine the changes or variations in Euler angles $[\theta, \phi, \varphi]$
- *Accelerometer*: as its name indicates, it is in charge of measuring the vehicle's acceleration. A malfunction of this sensor can lead to an incorrect vehicle's self positioning during flight.

6.3 Data retrieving

In order to analyze the data, parameters need to be first downloaded to the computer by either using an USB connection or a telemetry kit. It is remarkable that both methods work in a similar way with the only difference that the telemetry kit does not require any wire to carry out the data exchange, meaning that its usage is possible when flying. Since such device has not been installed on the vehicle, the data acquisition will be performed through an USB connection with logs. These logs are created based on the user preferences, which means that Mission Planner offers the possibility of selecting the data to be recorded into the processor's memory. However, since the needed data is basic information, no further action on our side is needed.



(a) Log accessing



(b) Log downloading

Figure 6.3.1: Data retrieving

6.4 Logs analysis

Once the logs are stored into the computer, they can be reviewed in Mission Planner to obtain the desired graphs¹. As it can be seen from Figure 6.4.1 the software's interface is divided in three parts. On the bottom part, the data is stored in two different ways: on the left it is organized by time and on the right all the information concerning the same parameter is stored and labeled. On the top part the selected parameters are plotted with respect to time.

¹www.copter.com/logs/analysis

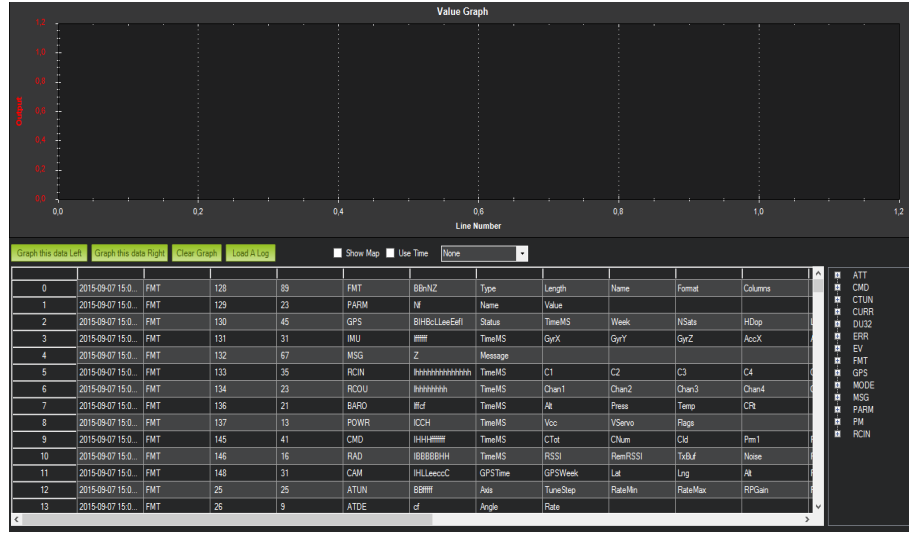


Figure 6.4.1: Logs interface

Although fourteen labels can be seen in the right side, only two of them will be used. However a short description of each of them is presented below:

1. *ATT*: it provides with the attitude information, the pilot's desired angles in centi-degrees and the vehicle's actual behavior.
2. *CMD*: it displays the commands received from the ground station as part of the mission.
3. *CTUN*: it shows the altitude records taken from the sonar and barometer and the climb rate.
4. *CURR*: it stores the battery current and voltage along with the board voltage information.
5. *DU32*: it specifies the 32bit integers or unsigned ones.
6. *ERR*: it gathers all the errors occurred during flight.
7. *EV*: it indicates every flight stage i.e. armed, takeoff, land...
8. *FMT*: it organizes Mission Planer column headers.
9. *GPS*: it discloses the number of satellite used and the measured altitude.
10. *MODE*: it enumerates the different modes used during flight.
11. *MSG*: it represents whether the messages received by the vehicle are successful.
12. *PARM*: it sets the parameters to be shown in the eeprom.
13. *PM*: it reveals the performance during flight
14. *RCIN*: it represents the transmitter electrical signals.

As mentioned above, in this case only two parameters are used: RCIN and ATT. From ATT the desired Euler angles are extracted and from RCIN the throttle's trend with respect to time is obtained. Afterwards, this data is inputted in Matlab by using the Simulink Signal Builder blocks for its subsequent processing.

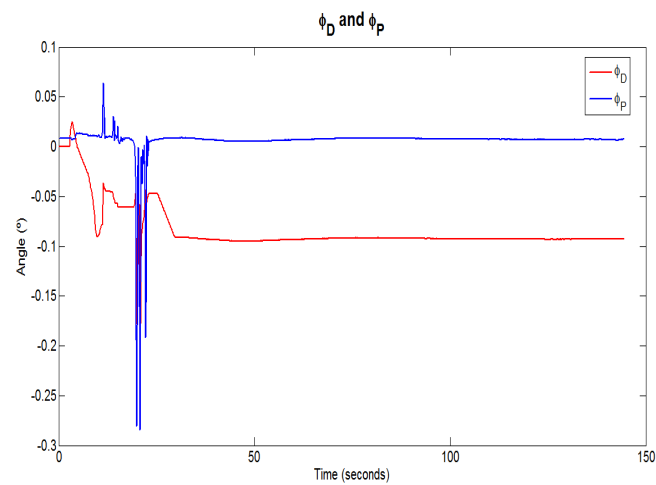
Chapter 7

Results

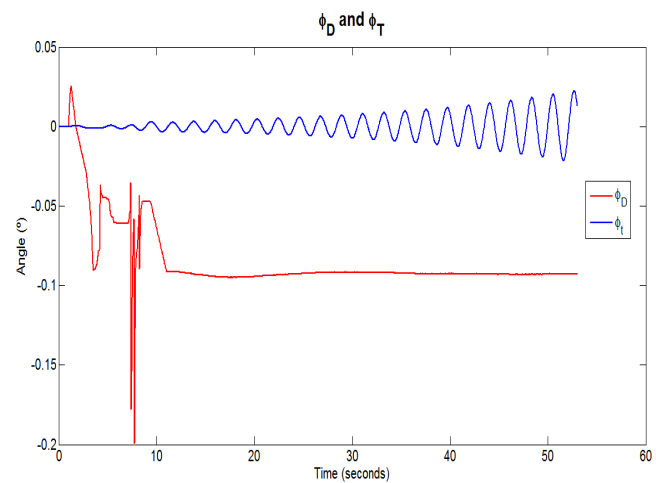
As it can be seen from Sub-Section 3.2.3 and Sub-Section 5.3.1 where the PID of both the vehicle and the theoretical model were tuned, the values do not coincide. Despite this dissimilarity, each set of parameters seem to fulfill their function. Consequentially, in order to clarify the reason to this phenomenon and to check that no error has been made two case scenarios are represented. On one hand, the PIDs obtained experimentally are inputted in Simulink and the real vehicle's behavior is compared against the model's one. On the other hand, the theoretical obtained PIDs are set in the vehicle through Mission Planner to compare the theoretical and experimental response.

7.1 Experimental PIDs in Simulink

In order to simulate the same scenario than the experimental one, the vehicle is first flown with the parameters that better stabilize it. Recalling Table 3.2 these values are $\phi_P = 0.164$, $\phi_I = 0.05$, $\phi_D = 0.004$, $\theta_P = 0.164$, $\theta_I = 0.085$, $\theta_D = 0.005$ and $\psi_P = 0.2$, $\psi_I = 0.002$, $\psi_D = 0$. Posteriorly, the processor is accessed through Mission Planner to download the transmitter commands and they are introduced in Simulink as the inputs. Moreover, the theoretical PIDs are changed to the above ones and the model is run. The outcomes of this system are the theoretical angles and the desired ones. From the graphs below the Mission Planner graphs and the Simulink one can be seen.



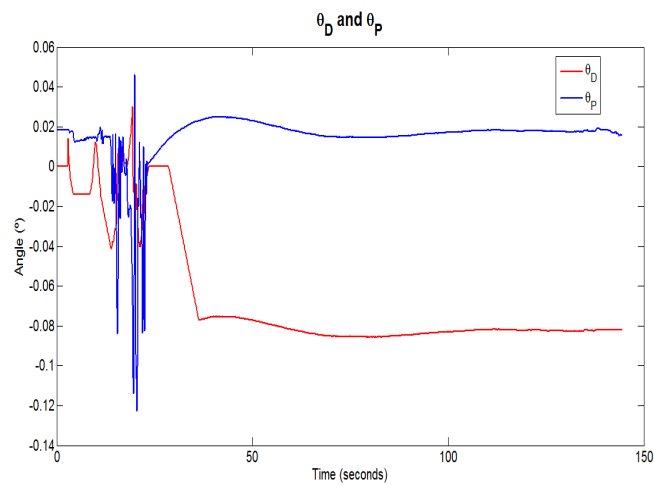
(a) Experimental



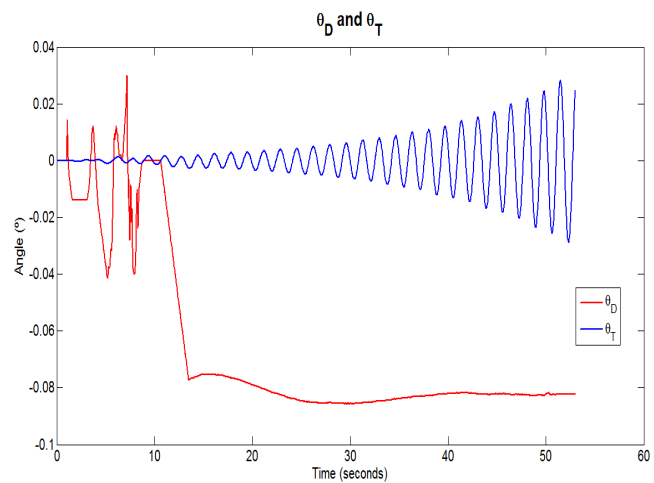
(b) Theoretical

Figure 7.1.1: Roll results

The first thing that is appreciated from the graphs is that the time scale does not coincide. This is due to the fact that Mission Planner starts counting for time when the APM is powered on. Beside this fact, it can be highlighted that while in the experimental graph both trends are similar, in the theoretical one the computed result diverges creating an oscillation out of control.



(a) Experimental



(b) Theoretical

Figure 7.1.2: Pitch results

It can be noticed from these graphs that both the experimental and theoretical outcomes are quite similar to Figure 7.1.1.a and Figure 7.1.1.b with the only difference that the period and amplitude of the divergence motion in the theoretical figure is bigger. This leads to the conclusion that in the y-axis the control will be lost within less time.

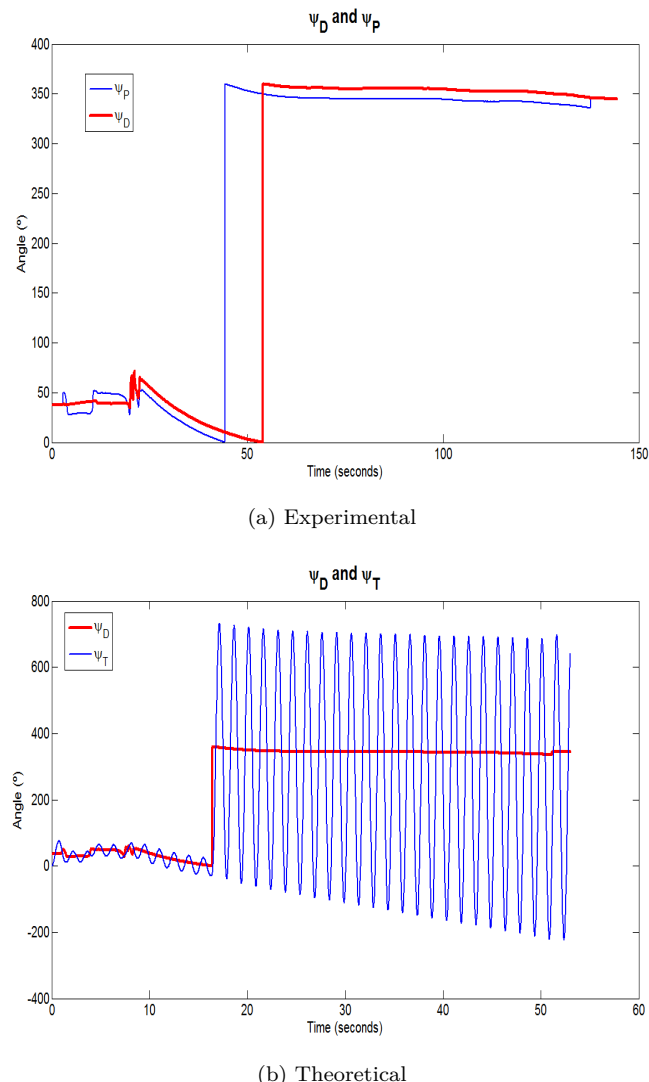


Figure 7.1.3: Yaw results

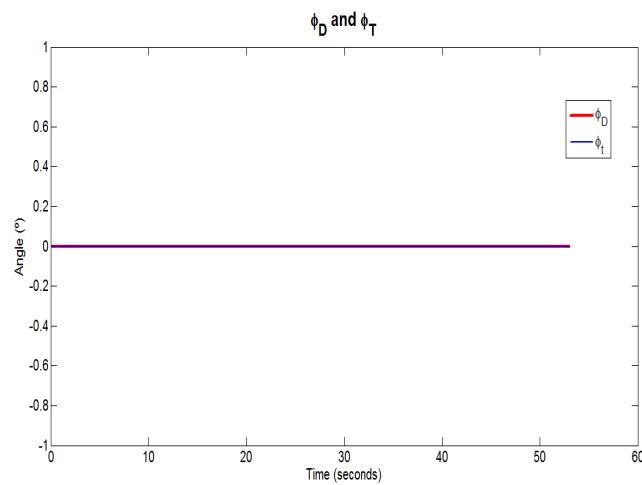
From these graphs, it can be seen that the outcome of the Mission Planner presents the same trend as the input but with a delay when the yaw is changed abruptly. Regarding the Simulink result, it concluded that these PID values lead to an uncontrolled motion in which the theoretical vehicle would rotate around itself 1400° in less than two seconds.

After analyzing the results from introducing the PID values obtained by manually tuning the vehicle with the transmitter into the dynamic model, it can be summed up that while these parameters are close to the ideal ones, to achieve a stable vehicle they only disturb the theoretical model. Thus they are unsuitable.

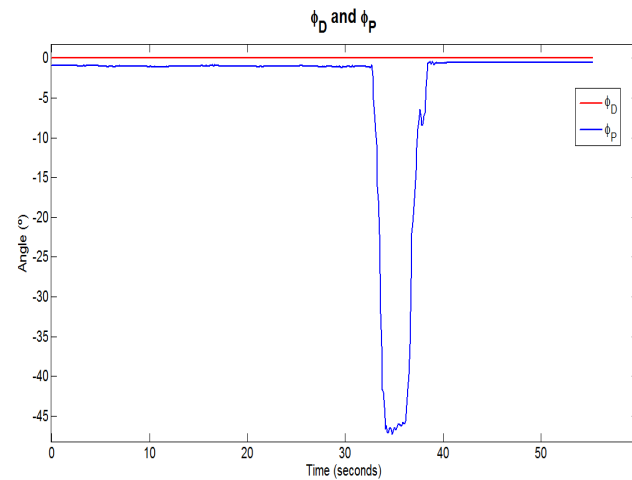


7.2 Theoretical PIDs in Vehicle

In this subsection, the opposite procedure as in the previous one is carried out. This means that the theoretical PIDs obtained in Sub-Section 5.3.1 are implemented in the real vehicle and both behaviors are analyzed. Therefore, it is expected to obtain similar trends of the desired angles and the output ones in the theoretical results. Since the vehicle will be subjected to different parameters from the ones that are believed to stabilize it, both roll and pitch transmitter inputs are maintained to zero in order to prevent the drone from flipping over and from damaging any crucial component.



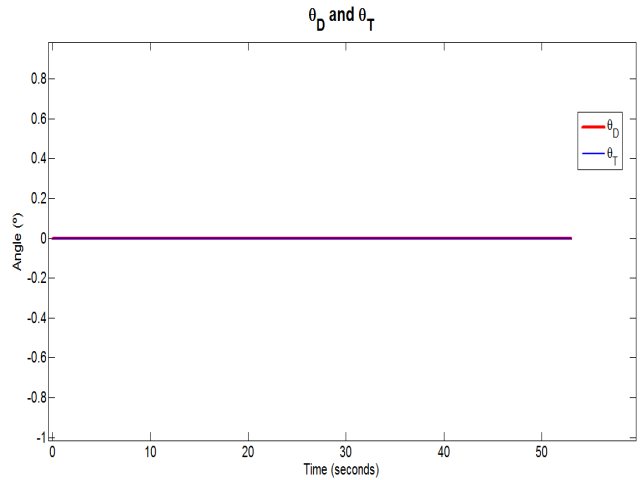
(a) Theoretical



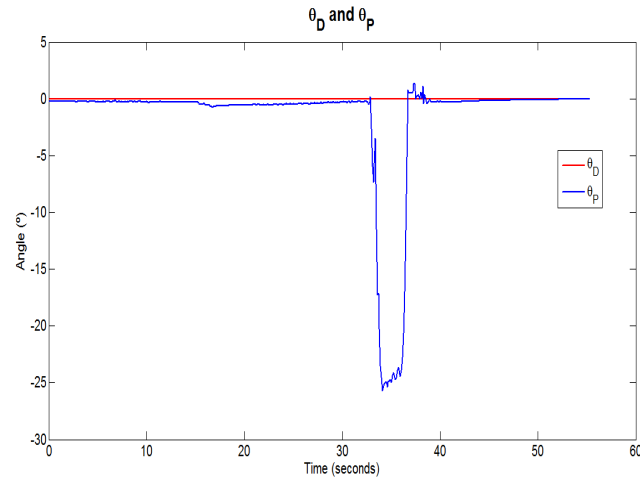
(b) Experimental

Figure 7.2.1: Roll results

As mentioned before and as it can be seen from Figure 7.2.1 the desired roll is set to zero. Furthermore it is appreciated that while the theoretical angle keeps being zero, the experimental graph shows that the vehicle rotates 45 degrees in the x-axis counter and clockwise sequentially in 3 seconds. This outcome indicates how abrupt and uncontrolled the movements are.



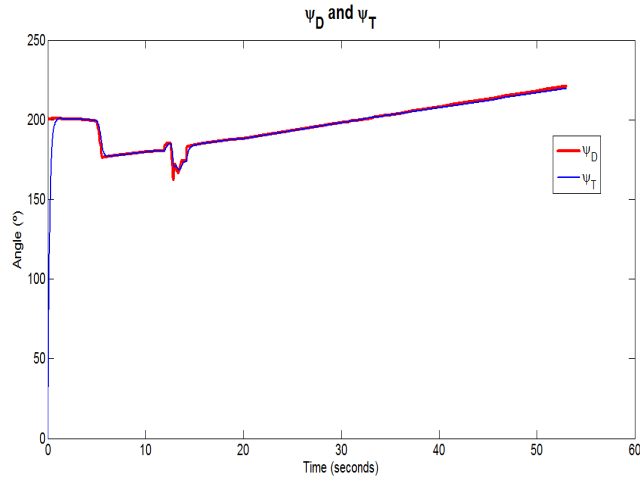
(a) Theoretical



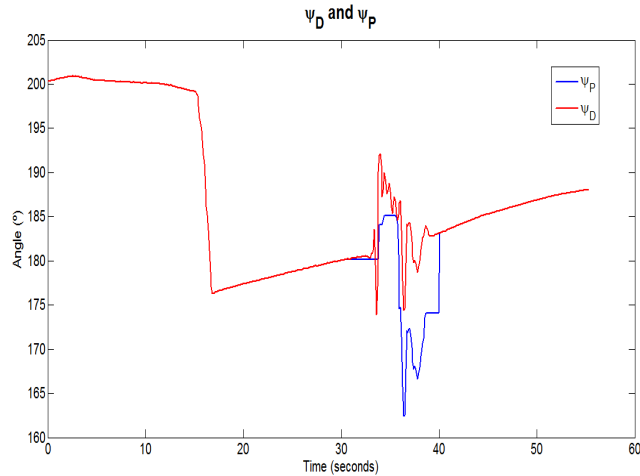
(b) Experimental

Figure 7.2.2: Pitch results

These two graphs do not differ much from the roll ones due to the high coupling that exists in these two movements. Moreover, it can be highlighted that the variation in pitch is less pronounced than in roll one as it rotates around 27° in three seconds. However this, it is still a dangerous motion that can lead to a loss of lift in one blade which could result in a crash.



(a) Theoretical



(b) Experimental

Figure 7.2.3: Yaw results

From Figure 7.2.3 it can be observed that the theoretical PID values make the theoretical outcome perfectly match the desired trend. Moreover, with respect to the Mission Planner plot is observed a maximum difference of 17° between the command and the vehicle's behavior.

After reviewing the obtained results from the vehicle's flight and the theoretical response to the same inputs it can be concluded that the used PIDs shall not be implemented under any circumstance in the drone as they provoke serious disturbances that lead to dangerous and uncontrolled lurches.

Chapter 8

Conclusions

Regarding the results presented in this bachelor thesis, several conclusions can be inferred. In order to conclude the project, a comparison between the objectives set at the beginning and the achieved ones is established:

The first goal was to find a vehicle that along with the appropriated components would best fit the mission requirements. This was translated into the selection of a robust DIY quadcopter with a open source processor that allowed me to introduce variants and improvements in its base code. Regarding the stabilization of the vehicle through the tuning of its controller, important improvements were introduced at the point of making possible a hover flight. Even though it was tried to be as accurate as possible, the tuning method is not infallible due to the trial and error nature of the process. Regarding the inertia characterization by using SolidEdge, we went one step farther, meaning that not only we did draw it but we printed it in 3D Appendix E which may mean that in the future we could print replacement parts. Moreover at the theoretical level, the dynamics of the quadcopter were successfully implemented in Simulink resulting in a powerful tool for the future once the vehicle is more stable. Once the results and comparison parts have been obtained and due to the dissimilarity observed between the two sets of PID parameters a meeting with an expert within this aeromodelism field is set up. During the reunion the whole process followed to construct the drone and its subsequent controller tuning is reviewed. The check up exposes the hereinafter stated anomalies:

1. Concerning the drone's processor it is highlighted that an excessive clamping to the upper frame plate along with the usage of a too hard foam cushion are interfering in the damping of the vibrations to which it is subjected.
2. Regarding the ESC's, their lose clamping wires are making the vehicle be non symmetric. This weight decompensation is translated into improper downward lurches towards the heavier side.
3. By reviewing the blades which are the most critical part of the vehicle it is observed that they are slightly unbalanced.
4. With respect to the vehicle's wiring it is noticed that a tighter clamping of the cables to the UAV's body would lead to a most accurate damping motion.
5. Concerning the soldering, it is checked that the used tin is used in plumbing applications. This is translated into an improper junction between the power distribution board and the electronic speed controllers which are in charge of powering up the UAV's processor.



6. With respect to the rope and sliding rods system used to fly the quadcopter indoors, it is seen that the tension of the wires contribute to great disturbances that unbalance the vehicle

Regarding the above listed effects, the expert concludes that errors 1 to 4 have low influence on the vehicle's behavior as they can be corrected through an optimum PID tuning. However, error 5 and 6 are related and more significant . On one hand, the soldering is introducing an undesired interference at the joint. In order to understand how crucial this interference is it has to be noticed that while on one hand, the purpose of materials used in plumbing applications is just bringing together two elements and preventing the appearance of leaks at the joint on the other hand the soldering required in the UAV field is responsible of acting as signals and commands transmitter. On the other hand the vehicle's sudden instabilities due to a bad transmission through the quadcopter's soldering are amplified by means of the elastic restoring forces of the flexible ropes.

8.1 Future work

Based on the present experience it is believed that introducing some minor changes could lead to a great improvement of the experiment. Moreover, these improvements are suggested as future work development:

1. The vehicle should be flown outdoors and untightened. Beside the unbalancing motion that the ropes introduce to the drone they also limit its maximum height accentuating the ground effect.
2. Regarding the vehicle's stabilization, it should be re done by using AutoTune. This mode attempts to tune automatically the PID parameters of the vehicle in order to provide with the highest response without overshoot. The methodology that it uses consists in abruptly change its angular rates to analyze the behavior while changing the PID values. Due to this, it is recommended to fly it outdoors in a controlled environment with high visibility.
3. Concerning the theoretical analysis, it is appreciated that a minimum error in the calculation of the drag and thrust coefficients has a great impact in the solution. Even though the measurements shown in Tables 10.1 and 10.1 were taken several times to avoid a possible error, it is recommended to recompute them in the future by using more precise tools.
4. With respect to the simulation, it is suggested to re-visit the Simulink files in order to implement a different controller, or even a non-linear one which may lead to an automation of the tuning process of the real vehicle.

Bibliography

- [1] *Boletín Oficial del Estado 17.10.2014*, number 252.
- [2] Jay Gundlach. *Designing unmanned aircraft systems: A comprehensive approach*. American Institute of Aeronautics and Astronautics, 2012.
- [3] Román Estebn Hofer. Preliminary design of an unmanned aerial vehicle with application to photovoltaic farm inspection. 2014/2015.
- [4] James Richard Wertz, David F Everett, and Jeffery John Puschell. *Space mission engineering: the new SMAD*. Microcosm Press, 2011.
- [5] Donald Norris. *Build your own quadcopter*. McGraw-Hill Education, 2014.
- [6] Samir Bouabdallah. *Design and control of quadrotors with application to autonomous flying*. PhD thesis, École Polytechnique federale de Lausanne, 2007.
- [7] Irfan Anjum Manarvi, Muhammad Aqib, Muhammad Ajmal, Muhammad Usman, Saqib Khurshid, and Usman Sikandar. Design and development of a quad copter (umaask) using cad/cam/cae. In *Aerospace Conference, 2013 IEEE*, pages 1–10. IEEE, 2013.
- [8] Robert C Nelson. *Flight stability and automatic control*, volume 2. WCB/McGraw Hill, 1998.
- [9] C Balas. *Modelling and Linear Control of Quadcopter*. PhD thesis, MS Thesis, Cranfield University, Cranfield, 2007.
- [10] Randal W Beard. Quadrotor dynamics and control. *Brigham Young University*, 2008.
- [11] Samir Bouabdallah, Pierpaolo Murrieri, and Roland Siegwart. Towards autonomous indoor micro vtol. *Autonomous Robots*, 18(2):171–183, 2005.
- [12] Samir Bouabdallah, Andre Noth, and Roland Siegwart. Pid vs lq control techniques applied to an indoor micro quadrotor. In *Intelligent Robots and Systems, 2004.(IROS 2004). Proceedings. 2004 IEEE/RSJ International Conference on*, volume 3, pages 2451–2456. IEEE, 2004.
- [13] Samir Bouabdallah and Roland Siegwart. Full control of a quadrotor. In *Intelligent robots and systems, 2007. IROS 2007. IEEE/RSJ international conference on*, pages 153–158. IEEE, 2007.
- [14] Gabriel de la Cal Mendoza et al. Modelado, simulación, construcción y control de un quadcopter. 2014.
- [15] Albert Garcia Junyent, Ana Maria Corraliza Jimenez, Rubén Recasens Orós, et al. Disseny, control i implementació d'un quadcopter. 2014.

- [16] Freddy Roberto Guerrero Noboa and Oswaldo Aníbal Menéndez Granizo. *Modelación, simulación y control de sistemas aéreos no tripulados utilizando inteligencia artificial*. PhD thesis, QUITO/EPN/2013, 2013.
- [17] ICAO. *Unmanned Aircraft System (UAS)*. International Civil Aviation Organization, 2011.
- [18] Shady A Kader, Adel-ezzat El-henawy, and AN Oda. Quadcopter system modeling and autopilot synthesis. In *International Journal of Engineering Research and Technology*, volume 3. ESRSA Publications, 2014.
- [19] Jon Larrañaga Fuerte. Experimentos de coordinación multi-robot con quadcopteros. 2014.
- [20] Xabier Legasa Martín-Gil. Cuadricóptero arduino por control remoto android. 2012.
- [21] Teppo Luukkonen. Modelling and control of quadcopter. *Independent research project in applied mathematics, Espoo*, 2011.
- [22] Vicente Martinez. Modelling of the flight dynamics of a quadrotor helicopter. *A MSc Thesis in Cranfield University*, 2007.
- [23] Yogianandh Naidoo, Riaan Stopforth, and Glen Bright. Quad-rotor unmanned aerial vehicle helicopter modelling y control. *International Journal of Advanced Robotic Systems*, 8(4):139–149, 2011.
- [24] VÍCTOR RAMOS VICEDO. *Diseño e implementación de un Quadcopter basado en microcontrolador Arduino*. PhD thesis, 2015.
- [25] Michael David Schmidt. Simulation and control of a quadrotor unmanned aerial vehicle. 2011.
- [26] Kimon P George J. Vachtsevanos Valavanis. *Handbook of Unmanned Aerial Vehicles*. Springer Reference, 2008.

Appendices

Appendix A

Aerodynamic Forces and Moments

In order to derive the dynamic model the Lagrange equation is utilized by taking into account the following assumptions:

- The structure is symmetric.
- The blades are rigid.
- Drag and Thrust are proportional to the square of the blade's angular velocity.

$$\begin{aligned} L &= T - V \\ \Gamma &= \frac{d}{dt} \left(\frac{\delta L}{\delta \dot{q}_1} \right) - \frac{\delta L}{\delta q_1} \end{aligned} \quad (\text{A.0.1})$$

where Γ are the forces, q_1 the coordinates, T the kinetic energy and V the potential energy. Taking the derivative of Equation 4.1.1 the corresponding velocities are obtained:

$$\begin{aligned} v_x &= -(sin\theta cos\psi \dot{\theta} - cos\theta sin\psi \dot{\psi})x + \\ &+ (-cos\psi cos\phi \dot{\psi} + sin\psi sin\phi \dot{\phi} - sin\phi sin\psi sin\theta \dot{\psi} + cos\psi cos\phi sin\theta \dot{\phi} + cos\psi sin\phi cos\theta \dot{\theta})y + \\ &+ (cos\psi sin\phi \dot{\psi} + sin\psi cos\phi \dot{\phi} - sin\psi cos\phi sin\theta \dot{\psi} - cos\psi sin\phi sin\theta \dot{\phi} + cos\phi cos\phi cos\theta \dot{\theta})z \\ v_y &= (-sin\theta cos\psi \dot{\theta} + cos\theta cos\psi \dot{\psi})x + \\ &+ (-sin\psi cos\phi \dot{\psi} - cos\psi sin\phi \dot{\phi} + cos\phi sin\psi sin\theta \dot{\psi} + sin\psi cos\phi sin\theta \dot{\phi} + sin\psi sin\phi cos\theta \dot{\theta})y + \\ &+ (sin\psi sin\phi \dot{\psi} - cos\psi cos\phi \dot{\phi} + cos\psi cos\phi sin\theta \dot{\psi} - sin\psi sin\phi sin\theta \dot{\phi} + sin\phi cos\phi cos\theta \dot{\theta})z \\ v_z &= (-cos\theta \dot{\theta})x + (cos\phi cos\theta \dot{\phi} - sin\phi sin\theta \dot{\theta})y + (-sin\phi cos\theta \dot{\phi} - cos\phi sin\theta \dot{\theta})z \end{aligned} \quad (\text{A.0.2})$$

The squared magnitude of the velocity is given by $v^2 = v_x^2 + v_y^2 + v_z^2$ allows the kinetic energy computation:



$$\begin{aligned}
T = & \frac{1}{2} \int y^2 + z^2(R)dm(r).(\dot{\phi}^2 - \psi)\dot{\phi}2\sin\theta + \dot{\psi}^2\sin^2\theta) \\
& + \frac{1}{2} \int z^2 + x^2(R)dm(r).(\dot{\theta}^2\cos^2\psi + \dot{\theta}^2\dot{\psi}^2\sin\phi\cos\phi\cos\theta + \dot{\psi}^2\sin^2\phi\cos^2\theta) + \\
& + \frac{1}{2} \int x^2 + y^2(R)dm(r).(\dot{\theta}^2\sin^2\psi - \dot{\theta}^2\dot{\psi}^2\sin\phi\cos\phi\cos\theta + \dot{\psi}^2\cos^2\phi\sin^2\theta) + \\
& + \int xy(R)dm(r).(\dot{\psi}^2\sin\phi\sin\theta\cos\theta + \dot{\psi}(\cos\phi\sin\theta\dot{\theta} - \sin\phi\cos\theta\dot{\phi}) - \cos\phi\dot{\theta}) \\
& + \int xz(R)dm(r).(\dot{\psi}^2\cos\phi\sin\theta\cos\theta + \dot{\psi}(-\cos\phi\cos\theta\dot{\phi} - \sin\phi\sin\theta\dot{\theta}) + \sin\phi\dot{\theta}) \\
& + \int yz(R)dm(r).(-\dot{\psi}^2\sin\phi\cos\phi\cos^2\theta + \dot{\psi}(\sin^2\phi\cos\theta\dot{\theta} - \cos^2\phi\cos\theta\dot{\phi}) + \sin\phi\cos\phi\dot{\theta}^2)
\end{aligned}$$

By assuming that the vehicle is completely symmetric the products of inertia are neglected. This assumption is confirmed by Table 4.2 which shows that the products of inertia are much smaller than the diagonal elements. This simplification leads to the following kinetic energy expression:

$$T = \frac{1}{2}I_{xx}(\dot{\phi} - \dot{\psi}\sin\theta)^2 + \frac{1}{2}I_{yy}(\dot{\theta}\cos\phi + \dot{\psi}\sin\phi\cos\theta)^2 + \frac{1}{2}I_{zz}(\dot{\theta}\sin\phi - \dot{\psi}\cos\phi\cos\theta)^2$$

The expression of the potential energy is:

$$V = g \int (-\sin\theta x + \sin\phi\cos\theta y + \cos\phi\cos\theta z)dm(r) = \int xdm(x)(-gsi\theta) + \int ydm(y)(gsin\phi\cos\theta) + \int zdm(z)(gcos\phi\cos\theta)$$

By applying the Lagrange equation, the equations of motion and small angle approximation the roll , pitch and yaw equations are found:

$$\begin{aligned}
\frac{d}{dt}\left(\frac{\partial L}{\partial \dot{\phi}}\right) - \frac{\partial L}{\partial \phi} &= \tau_\phi \\
\frac{d}{dt}\left(\frac{\partial L}{\partial \dot{\theta}}\right) - \frac{\partial L}{\partial \theta} &= \tau_\theta \\
\frac{d}{dt}\left(\frac{\partial L}{\partial \dot{\psi}}\right) - \frac{\partial L}{\partial \psi} &= \tau_\psi
\end{aligned}$$

Roll equation:

$$\ddot{\phi} = \frac{J_r\dot{\theta}(\Omega_1 + \Omega_2 - \Omega_3 - \Omega_4)}{I_{xx}} + \frac{I_{yy} - I_{zz}}{I_{xx}}\dot{\psi}\dot{\theta} + \frac{bl(\Omega_3^2 - \Omega_4^2)}{I_{xx}}$$

Pitch equation

$$\ddot{\theta} = \frac{J_r\dot{\phi}(-\Omega_1 - \Omega_2 + \Omega_3 + \Omega_4)}{I_{yy}} + \frac{I_{zz} - I_{xx}}{I_{yy}}\dot{\psi}\dot{\phi} + \frac{bl(\Omega_2^2 - \Omega_1^2)}{I_{yy}}$$



Yaw equation

$$\ddot{\phi} = \frac{J_r(\Omega_1^2 + \Omega_2^2 - \Omega_3^2 - \Omega_4^2)}{I_{zz}} + \frac{I_{xx} - I_{yy}}{I_{zz}} \dot{\phi} \dot{\theta}$$

Appendix B

Test bench data

Let the displayed weight on the scale be y and the angular velocity to the power of two be x . Both units are expressed in SI

x_i	y_i	$x_i * y_i$	x_i^2
2389188,49	0,33212	796077,6049	$5,70822*10^{12}$
2481885,16	0,40221	998239,0302	$6,15975*10^{12}$
2650709,61	0,41202	1092145,374	$7,02626*10^{12}$
2935739,56	0,44145	1295982,229	$8,61857*10^{12}$
3171961	0,46107	1462496,058	$1,00613*10^{13}$
3752743,84	0,49050	1840720,854	$1,40831*10^{13}$
4014813,69	0,54936	2205578,049	$1,61187*10^{13}$
4360579,24	0,58860	2566636,941	$1,90147*10^{13}$
4640577,64	0,64746	3004588,399	$2,15350*10^{13}$
4709768,04	0,68670	3186684,665	$2,21819*10^{13}$
4972454,01	0,72594	3609703,264	$2,47253*10^{13}$
5113929,96	0,75537	3862909,274	$2,61523*10^{13}$
$\sum_1^{12} x_i = 45194350,24$	$\sum_1^{12} y_i = 6,49388$	$\sum_1^{12} x_i y_i = 25969274,79$	$\sum_1^{12} x_i^2 = 1,81385 * 10^{14}$

Table B.1: Data to obtain C_T

Let x_i be the torque τ and y_i be the angular velocity to the power of two



V_i	I_i	P_{in}	P_{out}	x_i	y_i	$x_i * y_i$	x_i^2
0,6	4,3	2,58	0,774	2389188,49	0,000500744	1196,3718	2389188,49
0,8	5,6	4,48	1,344	2481885,16	0,000853117	2117,3376	2481885,16
0,8	5,7	4,56	1,368	2650709,61	0,000840243	2227,2408	2650709,61
0,9	6,5	5,85	1,755	2935739,56	0,001024279	3007,017	2935739,56
1,1	7,9	8,69	2,607	3171961	0,001463784	4643,067	3171961
1,3	9,4	12,22	3,666	3752743,84	0,001892422	7191,775	3752743,84
1,5	10,8	16,2	4,860	4014813,69	0,002425513	9737,982	4014813,69
1,6	11,5	18,4	5,520	4360579,24	0,002643425	11526,864	4360579,24
2	14,4	28,8	8,640	4640577,64	0,00401077	18612,288	4640577,64
2,1	15,2	31,92	9,576	4709768,04	0,004412497	20781,835	4709768,04
2,3	16,6	38,18	11,454	4972454,01	0,005136553	25541,275	4972454,01
2,4	17,3	41,52	12,456	5113929,96	0,005508092	28167,998	5113929,96
$\sum_1^{12} x_i = 45194350,24$				$\sum_1^{12} y_i = 0,03071144$	$\sum_1^{12} x_i y_i = 134661,0516$	$\sum_1^{12} x_i^2 = 1,81385 * 10^{14}$	

Table B.2: Data to obtain C_D

Appendix C

Mass of the components

Components	Quantity	Mass (g)	Total mass (g)
Upper frame plate	1	36,9	36,9
Lower frame plate	1	68,6	68,6
Arms	4	49,7	198,8
APM	1	33,1	33,1
Motors	4	53,2	212,8
ESCs	4	23,3	93,2
Receiver	1	8,1	8,1
Propellers	4	7,8	31,2
GPS	1	83,3	31,2
LiPo battery	1	191	191
			Quadcopter total mass: 957g

Table C.1: Kit components

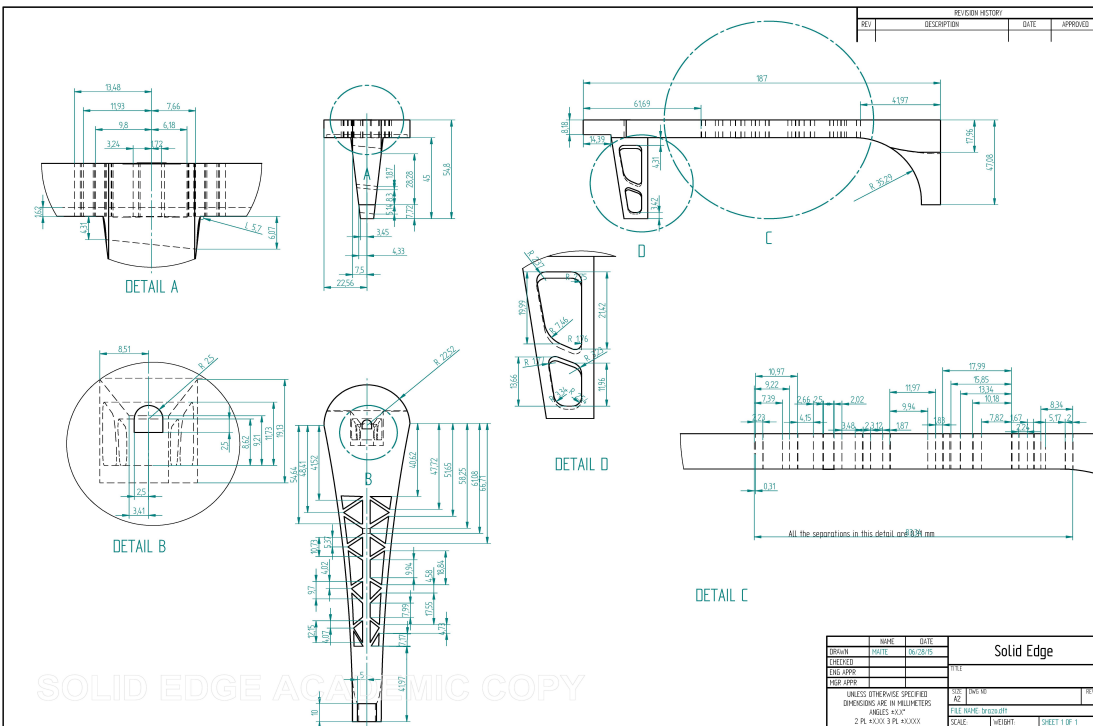
Appendix D

SolidEdge plans with dimensions

In the next three pages a draft of the non electronic components of the vehicle along with their measures will be displayed.

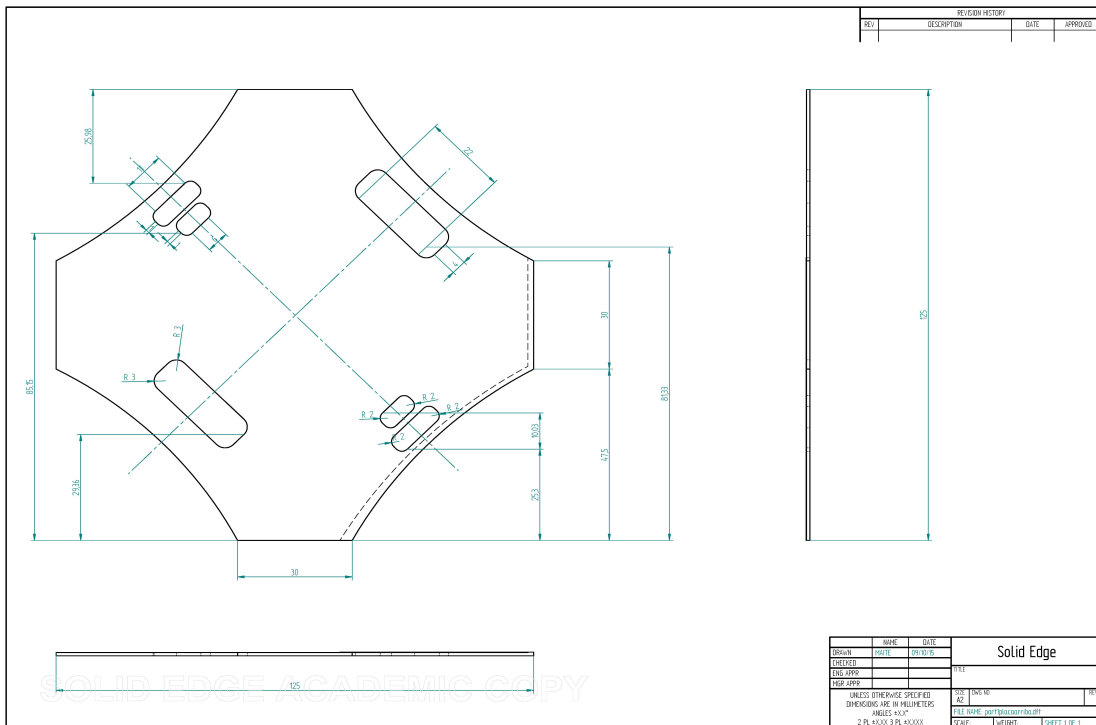


D.1 Draft of arm



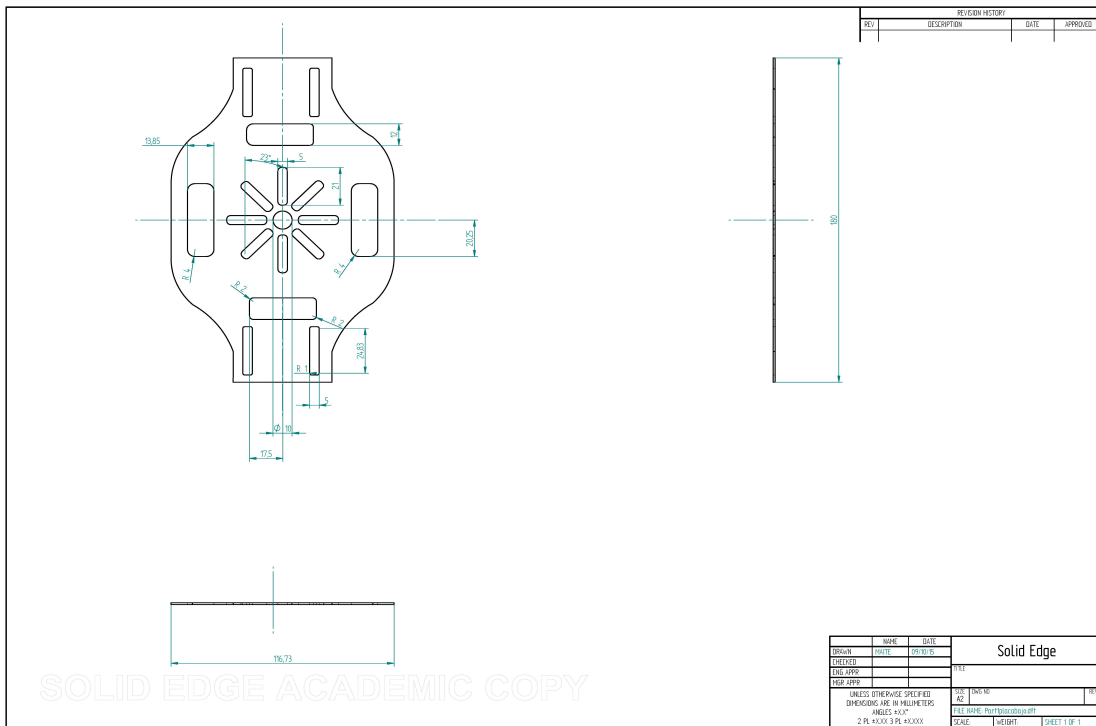


D.2 Draft of upper frame board





D.3 Draft of lower frame board



Appendix E

3-D printing

In *Sub-Section 4.5.1* it has been seen that the full model was modeled into SolidEdge for obtaining the moments of inertia. Furthermore it will used in two more applications: 3-D printing and simulation (*Chapter 6*). 3D printing is an additive manufacturing process in which successive colored powder layers are laid down to make three dimensional objects. Sometimes and depending of the purpose of the printed object a hardening liquid can be applied to it in order to make it more resistant to impacts. Moreover some of the printers have the capability of reproducing the mass properties of the printed objects by varying their densities. Under these circumstances, it is evident to state that if a non electrical component of the vehicle but the blades was broken it could be replaced by a 3D printing of it. In any case blades will be replaced as these new pieces will always lack flexibility and the same ability to absorb impacts.

Towards the end of verifying whether this would be possible at all, a 1:3 scaled vehicle has been printed. Even though firstly it was wanted to print the very same vehicle, due to the printer's precision tolerances some regions of the components have been thicken up to a total distance of at least 2milimeters. Also, instead of printing the whole assembly together, some elements such as the blades have been printed separately to avoid printing everything again if only a piece was broken.

The translation of the file extensions from SolidEdge to one supported by the printed is carried out by SolidEgde and outputs one document and a note block one which contains the mass properties. Despite this properties, this file does not include the colors. Thus by using the 3D printer interface colors are reassigned and the logotypes of both the Aerospace Department (*Fig.49.a*) and the University (*Fig. 49.b*) are included to the arms.



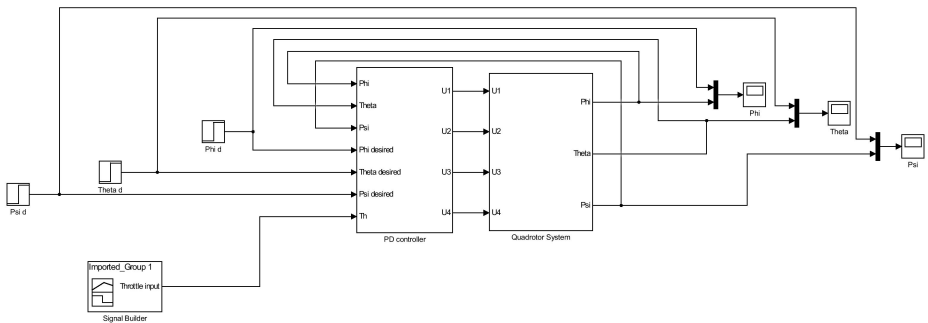
Figure E.0.1: Included logotypes



Figure E.0.2: 3D printed quadcopter

Appendix F

Simulink dynamic model



83

Figure F.0.1: Quadcopter Simulink model

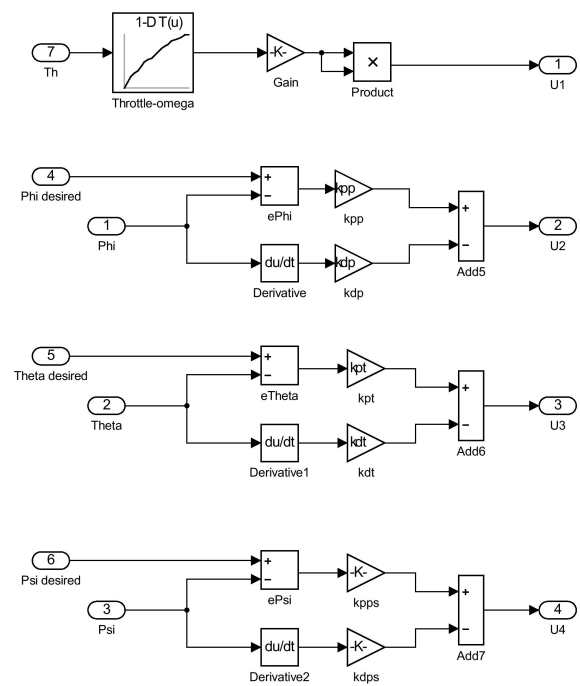


Figure F.0.2: PD controller

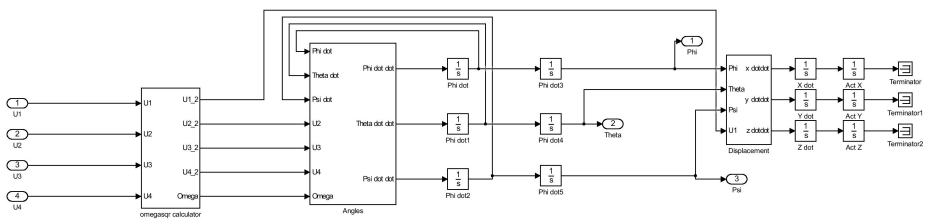


Figure F.0.3: Quadcopter dynamics



86

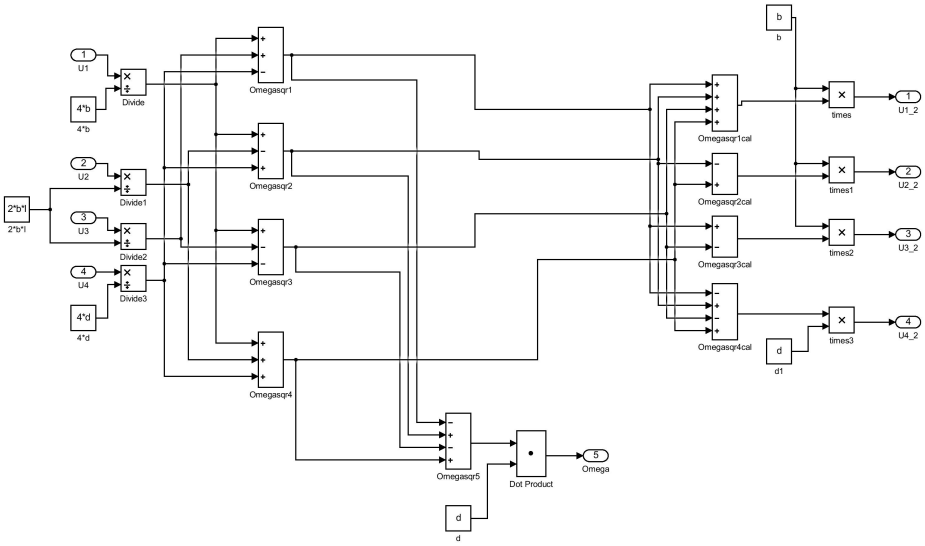


Figure F.0.4: Omega calculator block

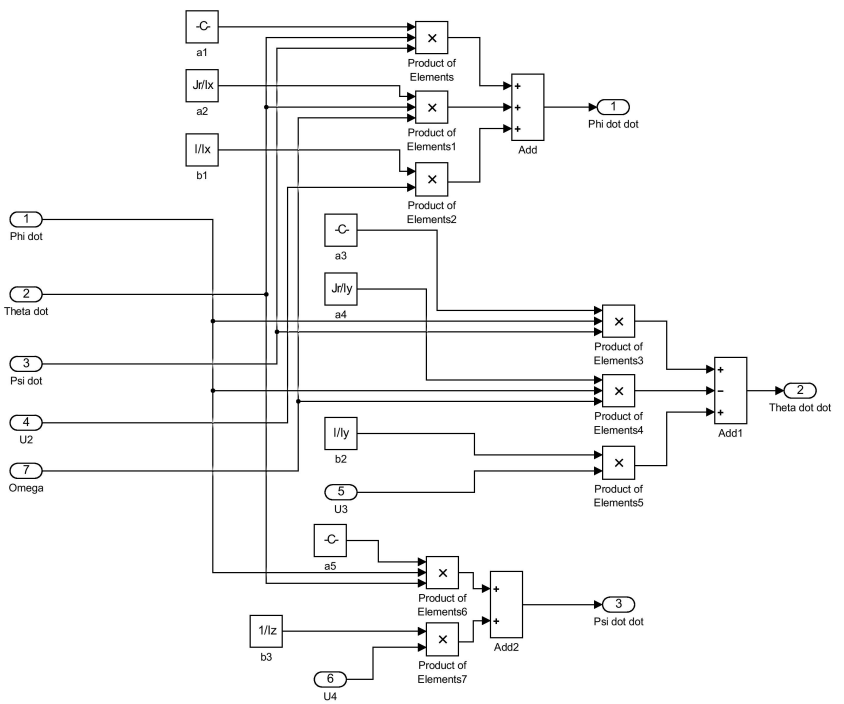


Figure F.0.5: Angle's block



88

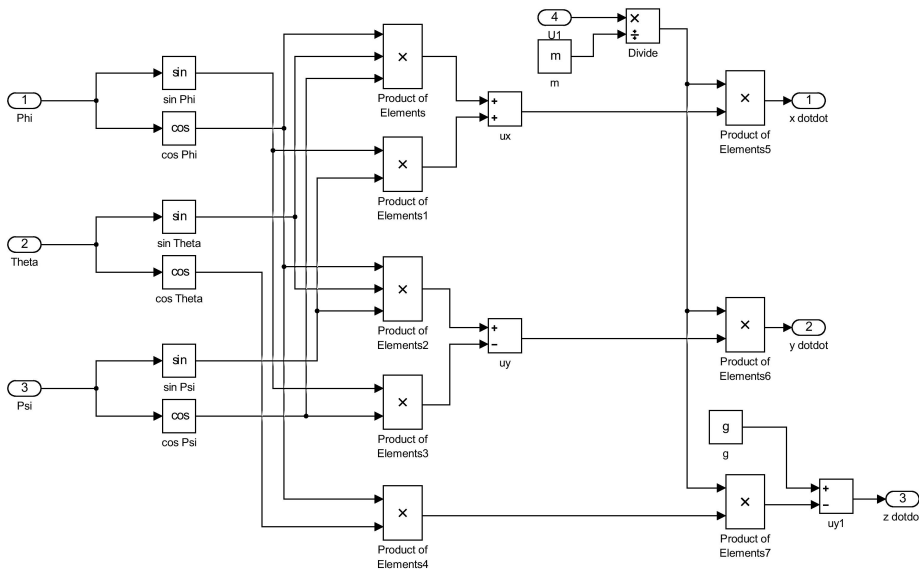


Figure F.0.6: Displacement block

Appendix G

Project budget

Materials			
Article	Price (€)	Quantity	Total(€)
Drone kit	301,64	1	301,64
Battery	15,62	1	15,62
			317,26

Additional structures			
Article	Price	Quantity	Total(€)
Test bench	20	1	20
Flying support	100	1	100
			120

Software			
Program	Version	License	Total (€)
Matlab and Simulink	R2012b	Student	124
SolidEdge	ST7	Student	0
Mission Planner	1.3.30	Free	0
			124€

Working hours			
Person	Number of hours	Price/hour	Total (€)
Student	560 hours	6	3360
Advisors	Visiting professor	56 hours	32.19
	PHD student	56 hours	13.95
			781.2
			5943.84

3D printing			
Piece	Volume (cm^3)	Price/ cm^3	Total (€)
Quadcopter	26.25	0.63	16.74
Blades	12.15	0.63	7.82
			24.56

The total price is 6529.66 €.